Robust pyrrole-Schiff base Zinc complexes as novel catalysts for the selective cycloaddition of CO2 to epoxides

Miguel Alonso de La Peña, Lynda Merzoud, Walid Lamine, A. Tuel, Henry Chermette, Lorraine Christ

Robust pyrrole-Schiff base Zinc complexes as novel catalysts for the selective cycloaddition of CO_2 to epoxides

Miguel Alonso de la Pena [a], Lynda Merzoud [b], Walid Lamine [b], Alain Tuel [a], Henry Chermette [b], Lorraine Christ [a]

[a] *Université de Lyon, Institut de Recherches sur la Catalyse et l'Environnement de Lyon, IRCELYON, UMR CNRS 5256, Université Lyon 1, 2 av. Einstein, 69626 Villeurbanne Cedex, France*

[b] *Université de Lyon, Institut des Sciences Analytiques, UMR CNRS 5280, Université Claude Bernard Lyon 1, Lyon, 69622 Villeurbanne Cedex, France*

A series of Zn (II) complexes with nitrogen Schiff base ligands (NSB) has been synthesized from pyrrole carboxaldehyde. The prepared complexes were fully characterized. Single crystal X-ray diffraction analysis showed various coordination modes, as monomers or as helical dimers according to the number of available nitrogen atoms surrounding the zinc cation. The complex structure optimizations were carried out using the density functional theory (DFT) with ADF program and the dimerization energies and the temperature effect were examined. The Zn complexes were used as Lewis acids (LA) combined with tetrabutylammonium halides (N_4BuX) as Lewis bases (LB), for the catalytic valorization of CO_2 into cyclic carbonates. A new momomeric Zn-NSB was chosen to study the influence of different reaction parameters (temperature, CO_2 pressure, LA/LB molar ratio, catalyst amount). Thus, optimized conditions afforded the solvent-free selective formation of styrene cyclic carbonate in good yields (up to 98 %) and allowed the reuse of this Zn-NSB/N_4BuX catalytic system without any loss of activity.

1. Introduction

One of the largest greenhouse gas emissions corresponds to carbon dioxide caused by anthropogenic actions. This undesirable excess of CO_2 makes it an abundant and inexpensive carbon source that, after fixation, can be used as C1 building-block [1–3], even if catalytic species may be used to overcome the thermodynamic stability of this molecule [4]. Thus, the insertion of CO_2 into epoxides may form polycarbonates or cyclic carbonates, in total atom economy reactions. Actually, the application field of cyclic carbonates is very large, from aprotic solvents as electrolytes in lithium ion batteries [5] to precursors for poly(carbonates) [6] and carbamates [7]. The cycloaddition of CO_2 into epoxides requires an acid-base catalytic system that usually consists in a cationic metal or an hydroxyl group as Lewis acid (LA) and a Lewis base (LB) such as an halide quaternary ammonium or phosphonium salt, or an ionic liquid [8–13]. The combined action of both catalytic centers is important to ensure the selectivity of the reaction towards cyclic carbonate; this occurs when the ring closing step in the mechanism [14] is promoted, thus avoiding the formation of polycarbonates (grey step in Scheme 1) [15]. One should notice the C…O tetrel bond in the intermediate. Let us recall that so-called tetrel bonds are non-covalent interactions between a molecule holding an atom of group 14 and an electron donor in another atom (or an anion or molecule) with lone electron pairs [16]. They stem from 'σ-holes' which are low electron density, (thus relatively positively charged), area adjacent to a σ-bonded element from groups 14. They are located along the same axis and on the opposite side of such atoms to the bond. These positive charges let the atoms act as Lewis acids, and bond non-covalently with electron donors. In in our case (Scheme 1), such C…O tetrel bond may be involved in the proposed intermediate. This tetrel bond formation is induced by an electrophilic attack by the carbon atom of a CO_2 substrate towards a nucleophilic oxygen atom of an epoxide. Recently, calculations have been performed to investigate some complexes of CO_2 with the azoles, evidencing tetrel bonds, hydrogen bonds and other secondary interactions [17].

A large number of Lewis acid-base catalytic systems has been reported, including heterogeneous systems, such as functionalized silica [18,19], MOFs [20–26] and supported complexes [27–30]. Studies of

* Corresponding authors.
E-mail addresses: henry.chermette@univ-lyon1.fr (H. Chermette), lorraine.christ@univ-lyon1.fr (L. Christ).

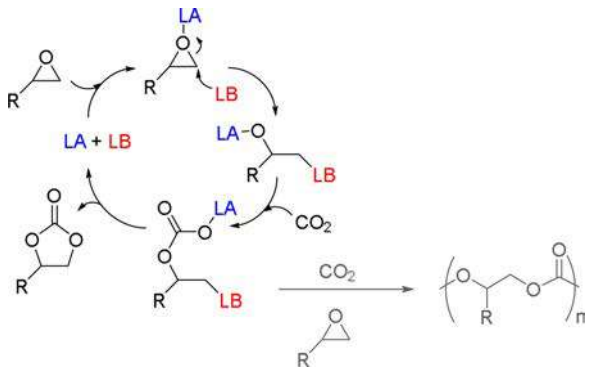

Scheme 1. Lewis acid/base insertion of CO_2 into epoxide mechanism.

homogeneous Lewis acid catalysts have been focused on the use of different metal (Cr, Mn, Fe, Co, Cu, Al…) complexes with modular ligands, such as the well-known salen ligands [31–35] which are N_2O_2 Schiff bases, or porphyrins which are planar N_4 ligands [36–38]. Nitrogen Schiff base (NSB) ligands have been developed combining the properties of both: the N_4 porphyrin-like coordinating sphere and the flexibility of the salen ligands open structure (Scheme 2) [39]. Some examples of NSB metal complexes derived from quinoline, pyridine, pyrrole or aniline aldehyde derivatives have been reported as catalysts for the CO_2 insertion into epoxides. Thus, a quinoline-based Cl-Fe-NSB complex was used as sole catalyst for the cyclic propylene carbonate synthesis, since the chloride atom on the coordination sphere acted as the Lewis base [40]. Later, a series of aniline-based Cl-Cr-NSB complexes were combined with tetrabutylammonium halides (NBu_4X) to give switchable catalysts for the synthesis of cyclic or polycarbonates, depending on the nature of the epoxide (terminal or not) and the complex (cationic or neutral) [41]. More recently, pyrrolidine-based Zn(II) complexes with NBu_4X were reported to catalyze the cycloaddition of CO_2 to 1,2-epoxyhexane (TON up to 2359 at 80 °C), using a Zn-complex to NBu_4I molar ratio of 1–2 [42]. Besides, some of us developed aniline-based Zn-NSB complexes which combined to NBu_4I in a 1/1 molar ratio, forms very active catalysts for the solvent free cycloaddition of CO_2 and styrene oxide (TON up to 4900 at 140 °C) [43]. This epoxide is a choice model substrate since it is a liquid easy to handle, and it is less reactive than the gaseous or volatile epoxides of industrial interest (ethylene and propylene oxide).

As Zn^{2+} is a Lewis acid cation with low toxicity able to form robust complexes with nitrogen ligands, we extended the scope of our study of zinc nitrogen Schiff base complexes using pyrrole instead of aniline aldehydes to form more stable species. Besides, the pyrrole derived Schiff base ligands synthesis is easier than the aniline analogs (no need to selectively reduce the nitro groups [39] and can afford to introduce a grafting group to allow their further grafting to silica supports.

Few examples of zinc-pyrrole based dimeric complexes were reported [44–47] but their use as catalysts for the cycloaddition of CO_2 was not investigated. Thus, we report here the synthesis and characterization of four stable pyrrole-derived Schiff base complexes (Scheme 3), two of them having central amine groups (**Zn-1**; **Zn-2**). The RX structure of three of them (**Zn-1**; **Zn-3, Zn-4**) were obtained and the catalytic properties of these four stable Zn-NSB complexes have been investigated for the selective valorization of CO_2 into cyclic styrene carbonate.

Only few papers report both the experimental and theoretical studies concerning zinc complexes as catalysts for the cycloaddition of CO_2 to epoxides [48]. The main objective of the present work is to assess the use of quantum chemical computations to predict the energetic and structural properties of these complexes. Moreover, Mulliken atomic charges have been calculated for each zinc center and thus lead to the Lewis acid character of the metallic cations. These approaches may allow a structure/reactivity relationship. Besides, Density Functional Theory (DFT) has been applied to study the complexation process of nitrogen Schiff base ligands with Zn^{2+} cation.

In this context, from their optimized structures determined in a first step, we have compared the obtained DFT results with the available X-ray data and studied the energetics of the dimerization-monomerization process (Scheme 4).

2. Results and discussion

2.1. Synthesis and characterization of pyrrole-based Zn complexes

A series of four nitrogen Schiff base ligands (**L1**-**L4**,Scheme 4) were obtained by the condensation of pyrrole-2-carboxaldehyde and acyclic flexible triamines (**1** and **2**) or cyclic more rigid diamines (phenyldiamine **3** and *trans*-cyclohexyldiamine **4**). The corresponding zinc complexes (**Zn-1** to **Zn-4**) were synthesized by reaction with Et_2Zn in anhydrous THF at room temperature, under nitrogen atmosphere since this zinc precursor is air sensitive and basic enough to deprotonate the NH pyrrole moieties. X-ray suitable crystals were obtained for **Zn-1**, **Zn-3** and **Zn-4.** Complexes **Zn-3** and **Zn-4** were already prepared by different synthetic pathways, and the X-ray structure of **Zn-4** was previously reported [44,47,49]. The zinc complexation of all the nitrogen Schiff bases prepared in this study was confirmed by IR spectroscopy with *i)* the absence of the ν(N-H) stretching bands in the range of 3250-3000 cm^{-1} and *ii)* the shift to lower energies of the azomethine ν(N═C) stretching bands (Table 1).

In the particular case of **Zn-1**, the theoretical and experimental ^1H

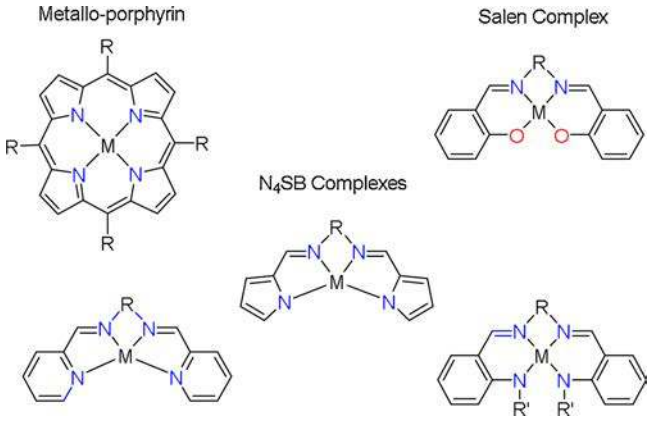

Scheme 2. Porphyrins and Schiff base complexes.

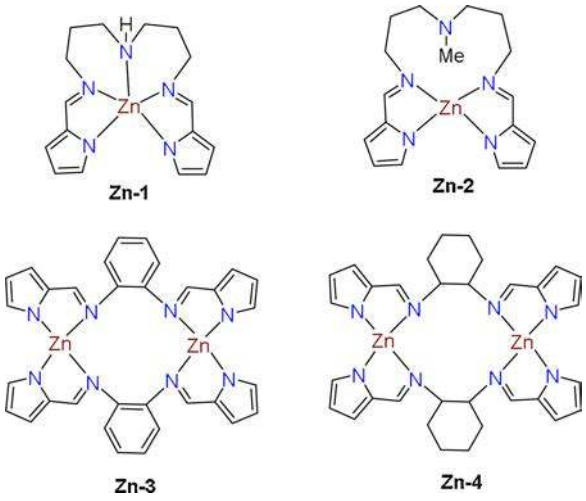

Scheme 3. Pyrrole-based Zn-NSB complexes.

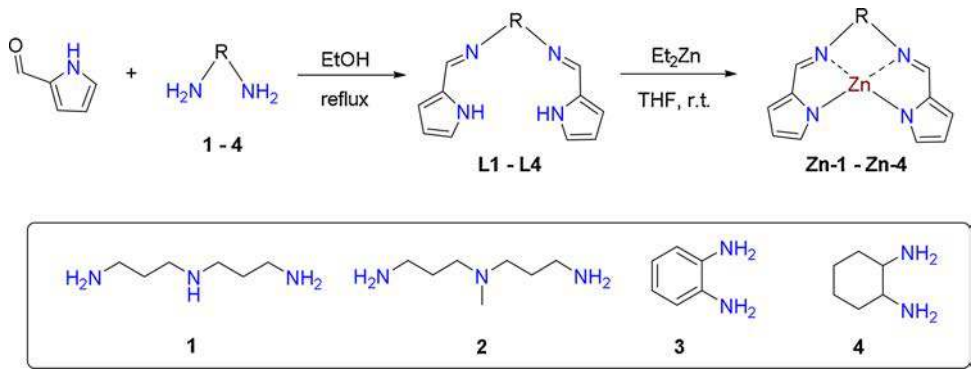

Scheme 4. General synthetic pathway of pyrrole-based Zn complexes.

Table 1
IR shift of N=C stretching bands in nitrogen Schiff base ligands and complexes.

	L1	Zn-1	L2	Zn-2	L3	Zn-3	L4	Zn-4
ν(N = C) cm^{-1}	1639	1602	1639	1591	1616	1551	1632	1591

NMR spectra suggests the presence of diasterotopic protons due to the zinc coordination of a fifth N atom, from the central amine group (Fig.1). The coordination of zinc center to the N central atom generates six-membered rings with a chair-like conformation that was also confirmed by the structure obtained from single-crystal X-ray diffraction and DFT analysis (Fig. 2 and Table 2). In the theoretical spectra each proton has a specific chemical shift, while in the experimental spectra, analog protons (*eg.* H6 and H10) in each chair conformation give a common signal as a multiplet.

The three N atoms of the central triamine are located at equivalent distances from the zinc center (~2.13 Å) while the two N atoms from the pyrrole moieties are little closer (~2.01 Å). The Zn^{2+} cation is coordinated to both nitrogen atoms of the imines (N2 and N16 in Fig. 2) in axial positions, while the three equatorial N atoms correspond to both pyrrole rings (N5 and N19) and the central amine atom (N12). Thus, **L1** is an N_5 ligand leading to a monomeric pseudo trigonal bipyramidal complex **Zn-1** where zinc has a formal valence electron number of 20, which is often found for this very late transition metal [43,50]. The

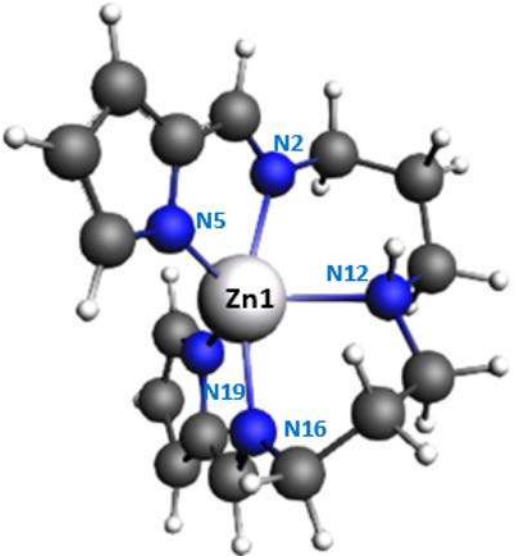

Fig. 2. Crystal structure of **Zn-1**.

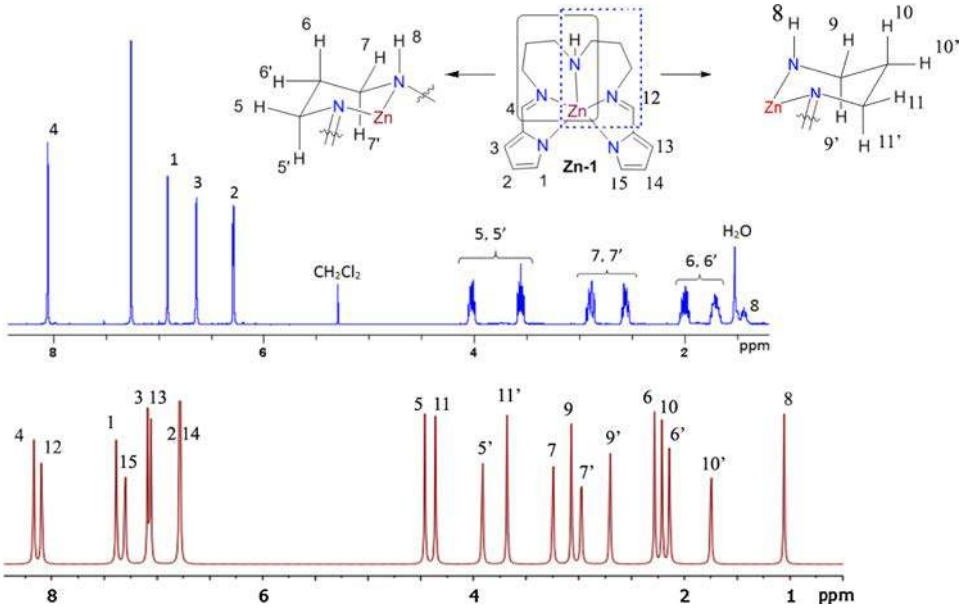

Fig. 1. ^{1}H NMR experimental in $CDCl_3$ (blue) and theoretical (red) spectra for **Zn-1**.

Table 2
Selected bond lengths and angles for **Zn-1** complex.

Bond lengths (Å)					
	Exp.	DFT		Exp.	DFT
Zn_1-N_{19}	2.006(59)	2.018	Zn_1-N_{12}	2.129(55)	2.329
Zn_1-N_5	2.026(52)	2.021	Zn_1-N_{16}	2.136(50)	2.158
Zn_1-N_2	2.125(47)	2.166			
Bond angles (deg.)					
N_{19}-Zn_1-N_5	119.6(214)	122.4	N_5-Zn_1-N_{12}	125.6(214)	125.2
N_{19}-Zn_1-N_2	103.7(220)	104.2	N_5-Zn_1-N_{16}	102.8(193)	102.7
N_{19}-Zn_1-N_{12}	114.8(211)	114.6	N_2-Zn_1-N_{12}	88.9(219)	88.5
N_{19}-Zn_1-N_{16}	81.7(221)	81.4	N_2-Zn_1-N_{16}	171.6(184)	171.2
N_5-Zn_1-N_2	80.3(199)	80.5	N_{12}-Zn_1-N_{16}	82.9(195)	82.9
N2-Zn-N5+ N5-Zn-N16+N16-Zn-N19+ N19-Zn-N2 = 368.6 deg. (360)					

distortion of the trigonal bipyramid is revealed by smaller bond angle values (with respect to purely symmetric shapes, see Table 2) for some angles, as between the axial atoms N2-Zn-N16 = 171.6 deg. or axial/equatorial ones, except for N2-Zn-N19 which has a value increased from 90 to 103.7 deg. Moreover, the presence of a fifth coordination on the zinc center stabilizes the complex as a Zn-N_5 monomer, avoiding the self-assembly of Zn(II) tetranuclear nitrogen Zn-N_4 species, as observed for **Zn-3** and **Zn-4** among others (Fig. 3).

The **Zn-1** complex optimization has been carried out at PBE/TZP level of theory with ZORA correction (BPE is Perdew-Burke-Ernzerhof exchange-correlation functional, TZP is triple zeta basis set with 1 polarization function, and ZORA is zero-order relativistic approximation). Some calculated bond lengths and angles of the complex, reported in Table 2 are compared to their experimental counterparts. As illustrated in Table 2, the obtained geometries confirm the fifth coordination of the zinc atom formed with the central N of the triamine ligand, in good agreement with X-ray geometries. Both N2 and N5 atoms of the imine and pyrrol groups are located at equivalent distances from the zinc cation (2.16 Å and 2.02 Å *cf.* Table 2). Finally, the fifth axial Zn-N bond is slightly larger (2.33 Å) in accordance with a distorted trigonal bipyramid. The angle values causing the distortion of the square pyramid compare well with the experimental ones. The average absolute deviation of X-ray experimental data with respect to DFT calculated bond lengths and angles are 5.4 % and 16.9 %, respectively. Additionally, the fifth coordination of **Zn-1** complex is confirmed by a very close to planarity of the angle around the zinc atom. These results indicate that this level of theory lets reproduce satisfactorily the X-ray structure.

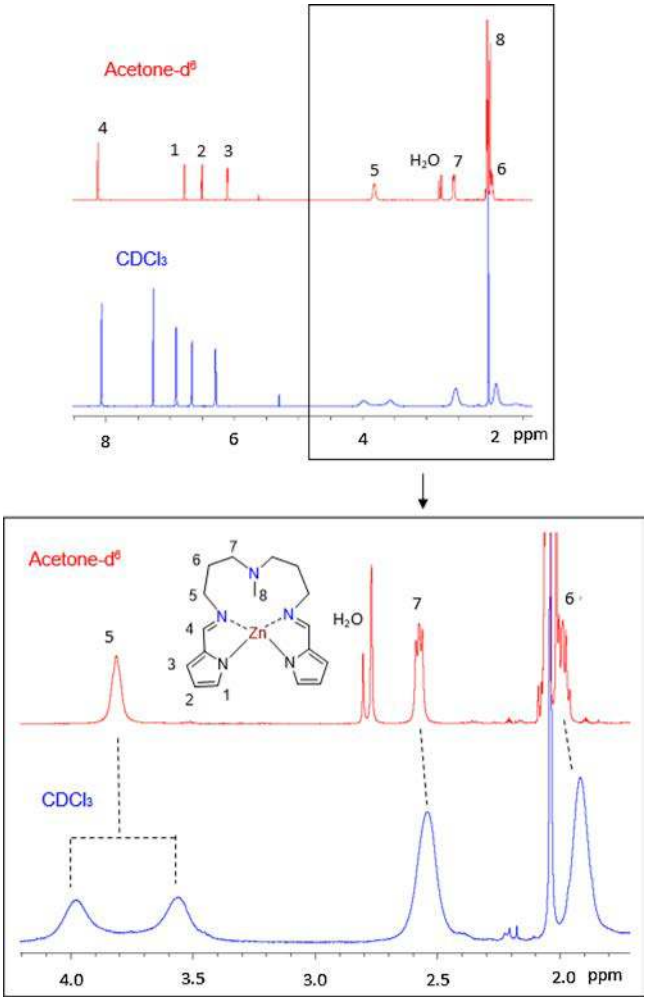

Fig. 3. ^{1}H NMR spectra for **Zn-2** in $CDCl_3$ (blue) and acetone-d_6 (red).

Complex **Zn-2** was prepared using a triamine derived Schiff base ligand in order to attempt to avoid the fifth coordination with the central N atom. Despite the absence of suitable crystals, complex **Zn-2** was fully characterized by ^{1}H NMR, ^{13}C NMR and HR-MS (ESI), which confirmed a monomeric species. The solvent used for the ^{1}H NMR (Fig. 3), had a great influence on the spectra resolution: the sharp signals obtained in a coordinating solvent such as acetone-d_6 became broad in $CDCl_3$, for the aliphatic protons. In a non-coordinating solvent, a fast N coordination/decoordination process may occur leading to the simultaneous presence of two species: Zn-**2**-N_5 and Zn-**2**-N_4, respectively with or without diastereotopic signals (Fig. 4a). Thus, the Schiff base ligand can behave as a tetra- or penta-dentate ligand and the methyl group bonded to the central nitrogen atom in **L2** hinders its coordination to the Zn^{2+} cation. Besides, in the presence of coordinating species, such as acetone-d_6, the NMR spectrum shows well-defined signals (red spectrum in Fig. 3) resulting from the oxygen atom (of the acetone molecule) coordination, instead of the central nitrogen atom of **L2**. In the acetone containing complex (Fig. 4b), the aliphatic protons cannot adopt a chair-like configuration and no diastereotopic signals can be observed.

Additionally, the theoretical chemical shifts of the protons in **Zn-2**-N_4 and **Zn-2-** N_4O complexes were determined and the resulting ^{1}H NMR spectra are given in Fig. 5. The NMR spectra show a difference in chemical displacements by changing the conformation. Thus, the difference between the observed chemical shifts is due to the fifth coordination with the oxygen atom of the acetone and to the loss of the chair configuration of the aliphatic protons.

The substitution of the hydrogen atom by methyl group in the central nitrogen atom prevents the fifth Zn coordination in this complex. The NBO results show that the three orbitals forming the **N2** bonds are hybridized: $sp^{2.68}$, $sp^{2.64}$ and $sp^{2.69}$ with CH_3 cf. Supplementary Information Table S.2. The contribution of each atom in the bonding orbital is 38 % for C and 61 % for N. In addition, these results show that the nitrogen lone-pair is mainly a nitrogen p orbital, as expected. The NBO results for Zn-**1** complex show that the nitrogen atom hybridizations are $sp^{2.65}$, $sp^{2.63}$ and $sp^{3.58}$ with H *cf.* Table S.2.

The structure of **Zn-1** and **Zn-2** complexes evidences the flexibility of the central dipropylamino bridge. As can see in Table 4 and Fig. 6, several conformers can be found for **Zn-1** and **Zn-2**. The most stable structure of these conformations of **Zn-1** and **Zn2** converged towards a structure with a pentacoordination of the Zn atom. (The Zn-N distances are given in Tables 2 and 3). In **Zn-1**, the fifth bond between the Zn atom and amino group involves the nitrogen lone pair, and the distance is similar to the lone pair bonding in the (tetrahedral) helical N4-Schiff-Base Zn(II) complex studied in ref. [51]. Interestingly, when the amine is a tertiary one (with a methyl in **Zn-2**), the expected bond between the nitrogen lone pair and the Zn is strongly weakened. In all cases, however, the nitrogen has a sp3 structure towards the covalent bonds. As can be seen in Table S.1, and comparing the Zn-N distances on **Zn-1** and **Zn-2**, the effect of the presence of the methyl group (probably enhanced with bigger substituents), is to weaken the Zn-N bond with the central N atom.

In order to identify the chemical shift of the proton H8 associated to

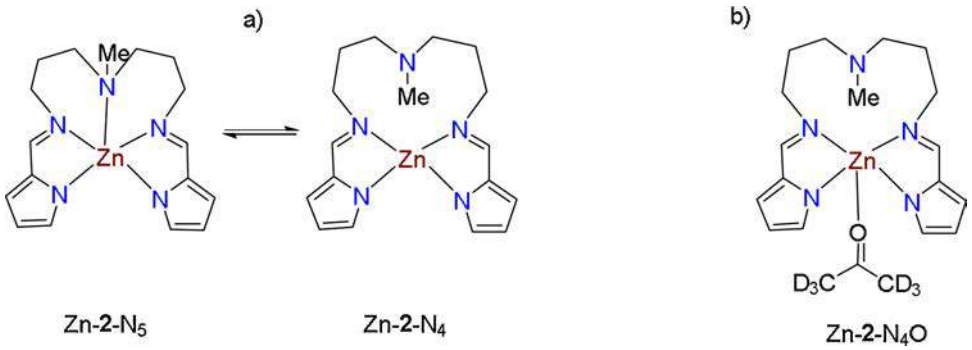

Fig. 4. a) **Zn-2** in $CDCl_3$: central N coordination/decoordination process b) **Zn-2** in acetone-d_6.

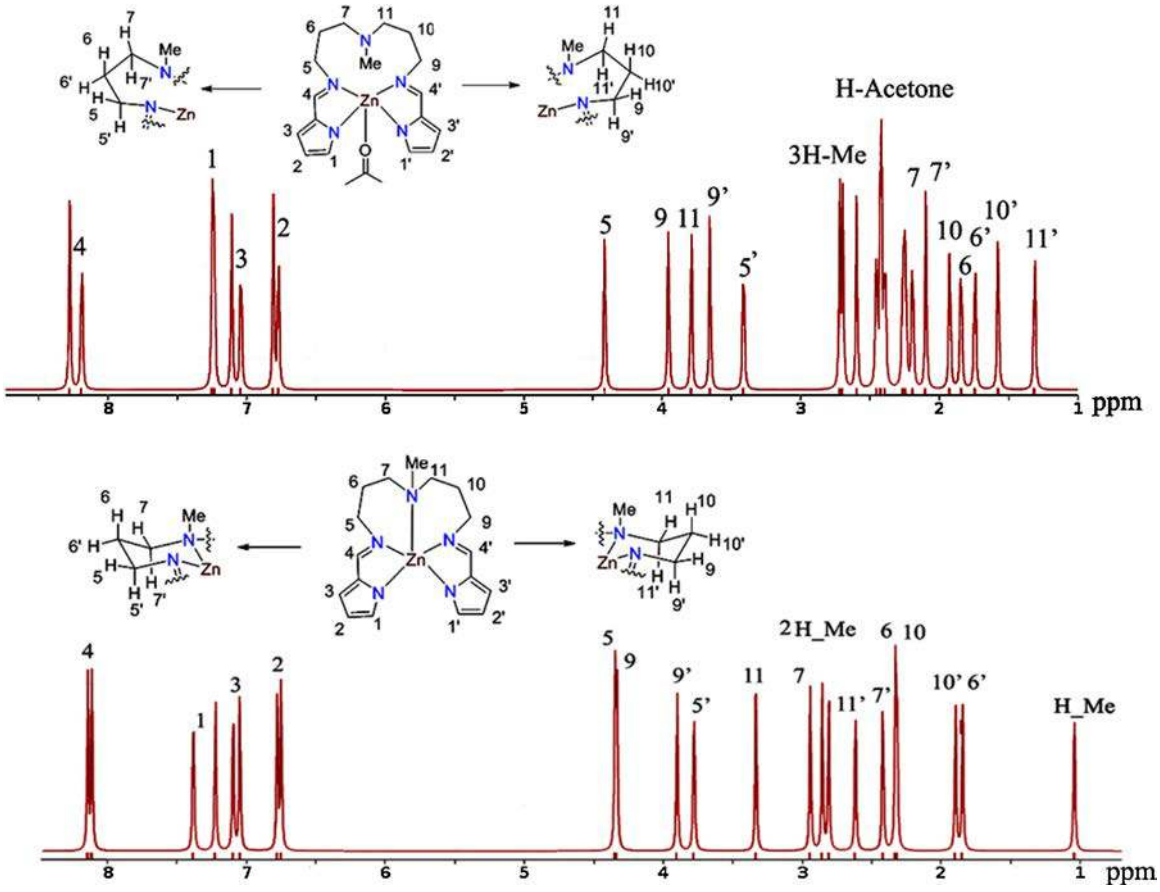

Fig. 5. ^{1}H NMR theoretical spectra for **Zn-2**-N_4 and **Zn-2**-N_4O.

the fourth and fifth coordination, the theoretical ^{1}H NMR spectra of the **Zn-1** complex and its different conformations, **Zn-1A** and **Zn1-B**, have been plotted in Fig. 7A. As can be seen in the obtained spectrum, the H8 proton chemical shift of the pentacoordinate **Zn-1** complex is located at 1.036 ppm. The NMR spectra of the tetra-coordinate Zn-1A and Zn-1B complexes have also been plotted on the same figure (c.f. Fig. 7A). The proton chemical shifts assessment of the ^{1}H NMR results obtained for the tetra- and penta-coordinate structures have been carried out. As can be seen in Fig. 7, the change from a fifth-coordinate to a tetra-coordinate complex causes a shift of the H8 proton signal towards higher ppm. In addition, this change in coordination causes a tilt of the aliphatic proton (H5, H6, H7, H9, H10 and H11) chemical shifts towards lower ppm. The chemical shift of the aliphatic protons towards the lowest ppm is characteristic of the change from the fifth coordinated species to the tetra-nitrogen coordination. This is related to the loss of the chair conformation of the amine chain.

The theoretical ^{1}H NMR spectra of different conformations of Zn-**2** complex are *also* given in Figs. 5 and 7. As well as for Zn-1 complexes, the Zn-2 conformations 1H NMR results show that the aliphatic protons (H5, H6 and H7) for Zn-**2**, which is very close to a Zn-N_5 complex, are shifted to lowest ppm values when moving to tetra nitrogen coordinated species Zn-**2A** and Zn-**2B**. According to the ^{1}H NMR results and the relative energy gap between Zn-**2** and its conformers (Table 4), we can assume an equilibrium between Zn-N_5SB and Zn-N_4SB species by changing their coordination mode.

The main purpose for the synthesis of complex **Zn-3** was to obtain a planar complex due to the conjugated pyrrole-phenyl Schiff base **L3**. The geometry of zinc complexes may greatly influence their Lewis acidic character [52–54], a higher acidity being obtained with a square planar geometry. In order to observe this influence, suitable crystals of **Zn-3**

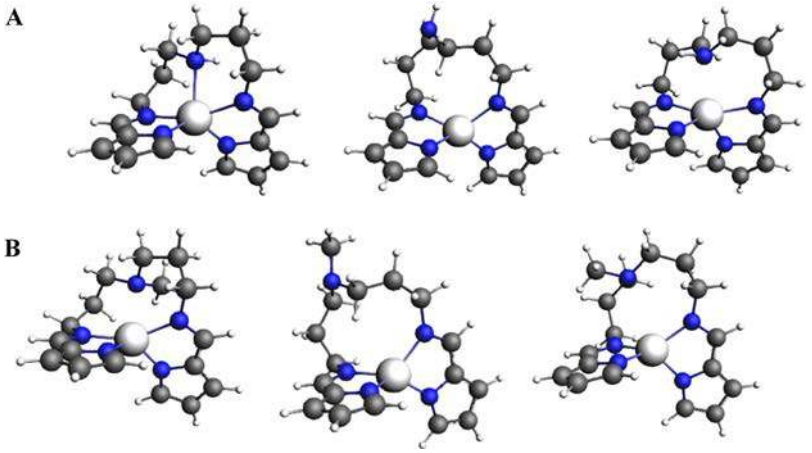

Fig. 6. The geometric structure of the **Zn-2** complex optimized at the PBE/TZP level with ZORA correction.
A. Some conformers of **Zn-1** complex
B. Some conformers of **Zn-2** complex

Table 3
Selected bond lengths and angles for Zn-2 complex.

	Zn-2 (DFT)
Zn-N_{20}	2.117
Zn-N_{23}	2.014
Zn-N_2	2.113
Zn-N_5	2.052
Zn-N_{16}	2.553
N_{23}-Zn-N_5	123.4
N_{23}-Zn-N_2	119.1
N_{23}-Zn-N_{16}	107.5
N_{23}-Zn-N_{20}	81.8
N_5-Zn-N_2	81.0
N_5-Zn-N_{16}	127.9
N_5-Zn-N_{20}	98.9
N_2-Zn-N_{16}	83.4
N_2-Zn-N_{20}	155.2
N_{16}-Zn-N_{20}	77.2

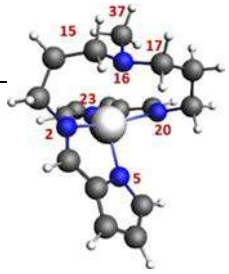

Table 4
A. Some conformers and nitrogen atoms selected bond lengths of **Zn-1** complex.

	Zn-1	Zn-1A	Zn-1B
Relative Energy (kJ/mol)	0.00	21.44	5.47
N_{16}-Zn	2.329	4.571	2.460
N_{16}-N_{20}	2.866	4.348	3.030
N_{16}-N_{23}	3.634	6.070	4.168
N_{16}-N_5	3.744	5.269	3.501
N_{16}-N_2	2.988	3.695	2.808
N_2-Zn-N_{20}	162.2	121.2	150.8

B. Some conformers and nitrogen atoms selected bond lengths of **Zn-2** complex.

	Zn-2	Zn-2A	Zn-2B
Relative Energy (kJ/mol)	0.00	10.83	0.05
N_{16}-Zn	2.33	4.66	3.31
N_{16}-N_2	2.99	3.75	3.04
N_{16}-N_{20}	2.87	4.40	3.40
N_{16}-N_{23}	3.63	6.16	5.02
N_{16}-N_5	3.75	5.36	4.07
N_2-Zn-N_{20}	162	119	131

were grown and characterized by X-ray diffraction (Fig. 8). Even if suitable crystals were obtained from ethanol solutions, no solvent coordination was observed and a dimeric helical species was formed, revealing pseudo-tetrahedral environment around zinc cations. Such result, similar to that obtained in some previous works [46,55] was indeed more or less anticipated and therefore did not surprise us. Selected bond lengths and angles are presented in Table 5: all N-Zn distances are similar and around 2 Å, and almost 3.5 Å distance is observed between the two zinc atoms. Nevertheless, bond angles for N1-Zn1-N5 = 146.8 deg. and N8-Zn2-N4 = 146.0 deg. show that the geometry is an intermediate between tetrahedral and square planar. Each Zn(II) is coordinated to two **L3** ligands, by means of one N pyrrole atom and one N imine atom. The dimer folds to give a self-assembly centrosymmetrical structure, avoiding the formation of the desired planar 18 electrons complex. Therefore, it seems difficult to obtain planar Zn(II) complexes due to their tendency to associate themselves in aggregates [54].

Racemic *trans* cyclohexyl diamine was used to prepare the **L4** Schiff base complex, and X-ray single crystal analysis of **Zn-4**, confirmed [47] a double-stranded helical structure, with a pseudo tetrahedral geometry for each zinc coordination. In our X-ray analysis, all Zn-N distances are close to 2 Å and the distance between the two zinc atoms is about 4 Å. The dimeric structure of this complex is quite similar to its phenyl analog **Zn-3**, but cyclohexyl moieties afforded chiral **Zn-4** single crystal with an M-(*R, R*) left-handed helicity in the asymmetric unit. The same trend was observed for a pyrrole-aniline Schiff base Zn(II) complex prepared recently in our group [51], which revealed to be quite unstable in non-anhydrous conditions.

As said previously, Zn-3 and Zn-4 complexes are crystallized as dimers, whereas the mechanism assumed for the catalytic reaction involves probably the monomers. This assumption holds on our experience on our previous studies on Zn-Sal(ph)en and N4-Schiff-Base Zn(II) complexes [43,51,52]. The monomer has also been shown to be the active catalyst in dimethyl carbonate synthesis from CO_2 and dimethoxytin(IV) complexes, preferably to the dimer [56,57]. A study of the detailed mechanism will be the subject of further work. Structural and thermochemical aspects of the complexation of **Zn-3** and **Zn-4** have been theoretically studied. Some bond lengths and angles of the dimer complexes and their calculated corresponding monomers are reported in Tables 5, 6 and 7 . On the structural level, the deviation between the calculated monomers value and formed dimers are also gathered in Tables S.4 and S.5. The calculated results of the average absolute deviation monomer/dimer of the bond lengths and angles respectively are 0.046 Å and 0.6 deg., for **Zn-3** and 0.013 Å and 1.1 deg. for **Zn-4**. These results indicate that the electrostatic and steric repulsion effects cause a rather small distortion of the valence angles forming the dimer structures. The comparison the **Zn-3** and **Zn-4** angles value was carried out *cf.* Table 7. The structure of monomer **Zn-3,** with phenyl, is perfectly flat while monomer **Zn-4** is not. This geometry deviation is due to the geometric deformation of the **Zn-3** monomer structure caused by the chair conformation of the cyclohexyl bridge.

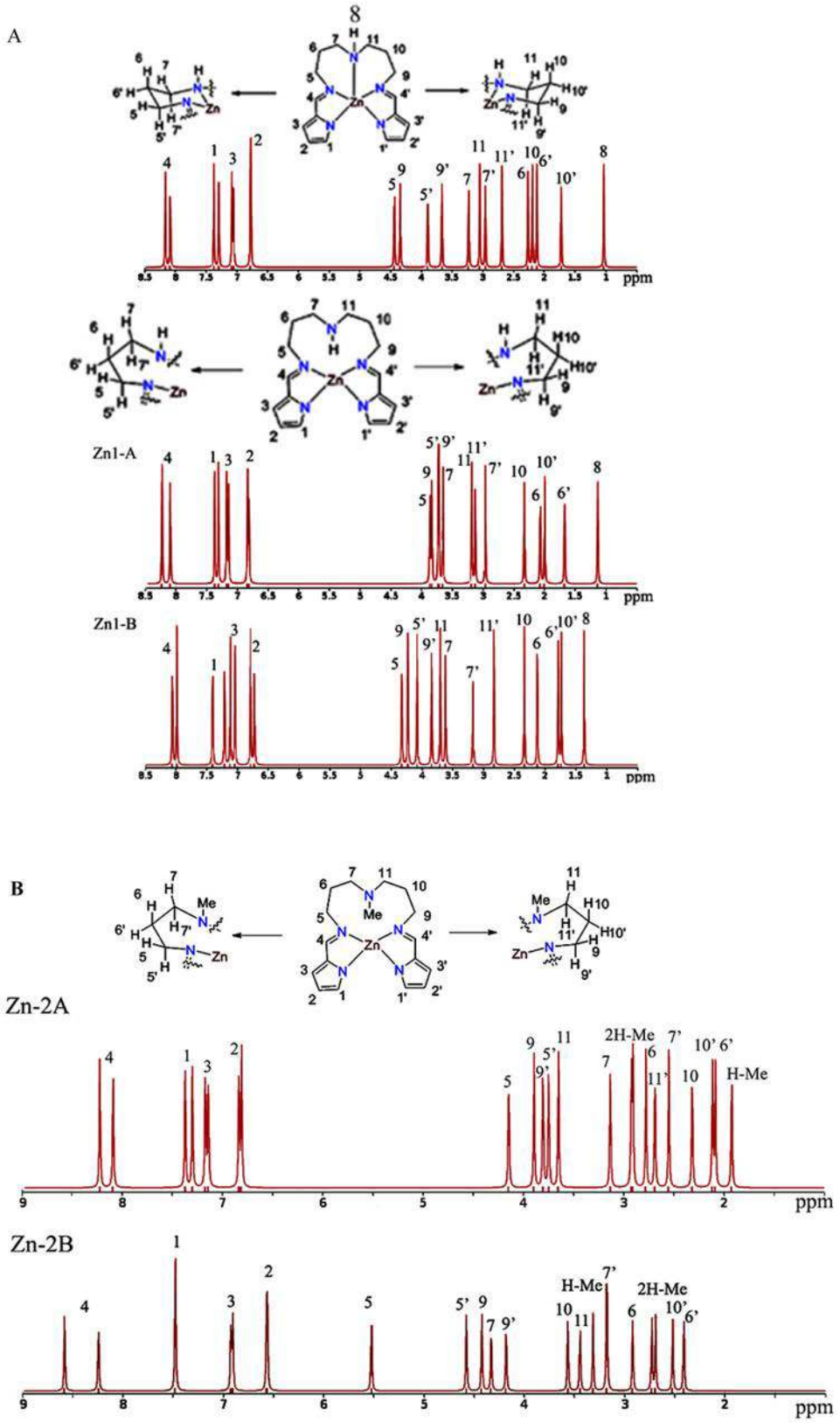

Fig. 7. A. ^{1}H NMR theoretical spectra for **Zn-1A** and **Zn-1B**.
B. ^{1}H NMR theoretical spectra for **Zn-2A** and **Zn-2B**

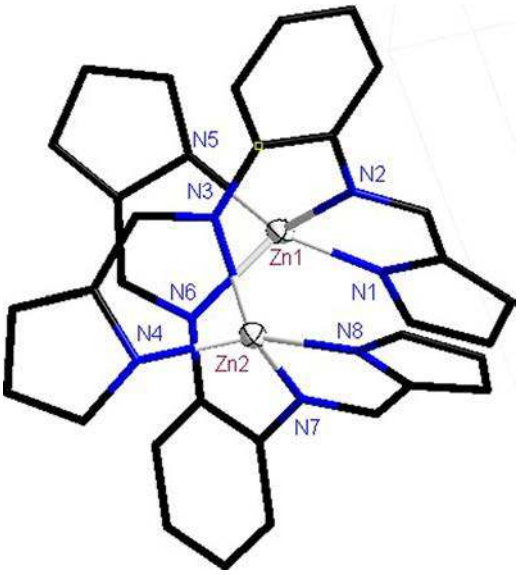

Fig. 8. Crystal structure of **Zn-3 (nitrogen: blue, carbon: black).**

Table 5
Selected bond lengths and angles for **Zn-3**.

Bond lengths (Å)					
	Exp.	DFT		Exp.	DFT
Zn_1-N_1	1.963(4)	1.984	Zn_2-N_8	1.948(4)	1.985
Zn_1-N_5	1.977(4)	1.984	Zn_2-N_4	1.970(4)	1.984
Zn_1-N_6	2.058(4)	2.079	Zn_2-N_3	2.048(4)	2.076
Zn_1-N_2	2.062(4)	2.078	Zn_2-N_7	2.057(4)	2.076
Zn_1…Zn_2	3.487(1)	4.079			
Bond angles (deg.)					
N_1-Zn_1-N_5	146.8(1)	139.0	N_8-Zn_2-N_4	146.0(1)	139.2
N_1-Zn_1-N_6	110.2(1)	116.2	N_8-Zn_2-N_3	114.4(1)	116.2
N_1-Zn_1-N_2	83.6(1)	84.5	N_8-Zn_2-N_7	83.5(1)	84.5
N_5-Zn_1-N_6	83.7(1)	84.5	N_4-Zn_2-N_3	84.4(1)	84.5
N_5-Zn_1-N_2	108.7(1)	116.6	N_4-Zn_2-N_7	107.9(1)	116.4
N_6-Zn_1-N_2	133.9(1)	120.2	N_3-Zn_2-N_7	127.4(1)	120.2

We have therefore optimized the geometries of Zn-3 and Zn-4 monomers, and calculated the free energy involved in the monomerization-dimerization process. The electronic dimerization energy is just the energy difference between the dimer energy and twice the monomer (PBE energies) energy. The free dimerization energy is the same, but it includes entropy terms and vibrational energy. As expected, the entropy favors the dissociation of the dimer, and reduces significantly the dimerization energy. The corresponding energies are reported in Table 8. From these values, two conclusions can be extracted:

1 The dimerization energy is quite small, so that one can expect that the equilibrium monomer-dimer can be easily displaced towards monomers if they are involved in the catalytic cycle, or towards dimers if the crystallization occurs. According to a previous work on N4SB Zn complexes [55,62] the probability that the catalytic process (cycloaddition of CO_2) occurs with the monomer (less hindered than the dimer to be approached by the reactants) is strong. In the present case, the monomer-dimer equilibrium should be easily displaced to the monomer via the consummation of the free monomer by the catalytic process.
2 The kinetics associated to the equilibrium has not been calculated. However, the influence of the temperature on the thermodynamics has been estimated, and one can see that the free energy difference between dimers and monomers increases by 18.8 kJ/mol in favor of the monomer, when the temperature moves from 293 to 373 K, an expected effect due to the enhancement of entropy of the monomers when the temperature increases (Table 8).

The accuracy of the DFT calculations is well-known to depend on the choice of the XC functional. Several benchmarks have been published which provide some confidence on given functionals for several classes of compounds, but these classes generally consist in organic or bio-organic systems. In case of organometallic systems, it is generally admitted that GGA functionals provide reliable results, whereas the inclusion of dispersion may shift some values. We tested some of them with the help of the "metaGGA" keyword in the ADF code. From the data obtained, one can estimate the accuracy of the energies in the 21−29 kJ/mol range. A similar conclusion was obtained in a study of a cavitand complex [59]. It is important to do that, because one often can see calculations performed with the default parameters provided by the Gaussian code, with no more control. From the Table S.5. given in the Supplementary Information, one can extract some more conclusions such as:

- Hybrid functionals provide dimerization energies a few kcal larger than the corresponding GGA (ex.: B3LYP *vs* BLYP, or PBE0 *vs* PBE, reported in Table 9). This can reasonably be attributed to the long-range interaction provided by the HF exchange.
- Dispersion corrected functionals lead to enhanced dimerization energies. This is expected since weak non covalent interactions are better taken into account. However, one should warn that the amount of dispersion energy included in the dispersion-corrected functional is parameterized for each functional, and therefore is functional-dependent.
- Some metaGGA or (hybrid metaGGA) functionals built with large numbers of fitted parameters (*e.g.* M05, M06,..) lead to unreliable results. This is in accord with the lack of polynuclear systems in the databases used for their parameterization.

In order to evaluate the Lewis acid character of the studied catalysts, the Mulliken charge analysis of the four zinc complexes previously prepared has been extracted from the calculations. As can be seen in Table 10, the zinc atoms of the **Zn-1** and **Zn-2** monomers have larger Mulliken charges than those of the two dimer species **Zn-3** and **Zn-4**. This is in agreement with a higher Lewis acid character that may lead to a better reactivity, which can be enhanced by the steric hindrance of the Zn within the dimers.

2.2. Catalytic Cycloaddition of CO_2 over styrene oxide using Zn(II) complexes

Pyrrole derived Schiff base complexes **Zn-1** to **Zn-4** were tested as homogenous Lewis acids (LA) catalysts in the cycloaddition of CO_2 over some epoxides in the presence of tetrabutylammonium halides, NBu_4X, as Lewis bases (LB). As this reaction can lead to cyclic carbonates or polycarbonates, its selectivity towards styrene cyclic carbonate (SCC) strongly depends on the combined nature of the Lewis acid and base catalysts. Reaction conditions may also have an influence on the cycloaddition selectivity, since cyclic carbonates usually are the thermodynamic products [14,60]. Styrene oxide (SO) was chosen as model substrate for the screening of reaction conditions, and the styrene cyclic carbonate (SCC) yields were determined by H^1 NMR using mesitylene as internal standard. The influence of the nature of Lewis acids, Zn-NSB complexes, and bases, NBu_4X was first examined (Table 11).

As already reported [61,62], tetrabutylammonium halides (X = Cl, Br, I) alone are able to catalyze the CO_2 cycloaddition to epoxides. In the conditions used here, they have similar activities leading moderate cyclic carbonate yields (Table 11, Entry 1: average values). Adding a Lewis acid as zinc complexes, improves both SO conversion and SCC yields, whatever the nature of the ammonium halide. Besides, the nature and structure of the Zn-NSB complex significantly influence the results.

Table 6
Selected bond lengths and angles for **Zn-4** (**DFT** calculation).

Distance (Å)					
	DFT	**Exp.**		**DFT**	**Exp.**
Zn_1-N_3	2.078	2.063	Zn_2-N_8	1.985	1.970
Zn_1-N_9	1.984	1.955	Zn_2-N_4	2.076	2.061
Zn_1-N_7	1.984	1.955	Zn_2-N_6	1.984	1.970
Zn_1-N_5	2.079	2.063	Zn_2-N_{10}	2.076	2.061
Zn_1-Zn_2	4.080	3.975			
Angle (deg.)					
	DFT	**Exp.**		**DFT**	**Exp.**
N_3-Zn_1-N_9	116.6	114.8	N_4-Zn_2-N_8	116.4	114.4
N_3-Zn_1-N_7	84.5	84.5	N_4-Zn_2-N_6	84.5	84.5
N_3-Zn_1-N_5	120.2	120.4	N_4-Zn_2-N_{10}	120.2	119.9
N_7-Zn_1-N_5	116.2	114.8	N_6-Zn_2-N_{10}	116.2	114.4
N_7-Zn_1-N_9	139.0	142.1	N_6-Zn_2-N_8	139.2	143.0
N_5-Zn_1-N_9	84.5	84.5	N_{10}-Zn_2-N_8	84.5	84.5

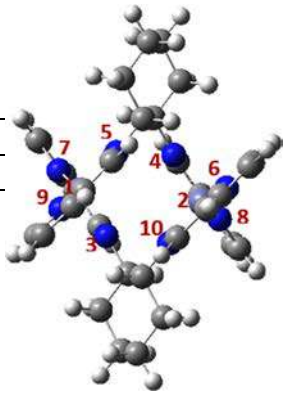

Table 7
Selected bond lengths and angles for Zn-3 and Zn-4 monomers (DFT Calculation).

Zn-3 Monomer		Zn-4 Monomer	
Distance (Å)		**Distance (Å)**	
Zn-N_1	2.143	Zn-N_1	2.114
Zn-N_2	2.143	Zn-N_2	2.113
Zn-N_3	1.994	Zn-N_3	1.975
Zn-N_4	1.995	Zn-N_4	1.974
Angle (deg.)		**Angle (deg.)**	
N_1-Zn-N_2	74.4	N_4-Zn-N_3	132.2
N_1-Zn-N_3	154.7	N_4-Zn-N_1	82.2
N_1-Zn-N_4	80.3	N_4-Zn-N_2	140.6
N_2-Zn-N_3	80.3	N_1-Zn-N_2	76.7
N_3-Zn-N_4	124.9	N_1-Zn-N_3	140.4
N_2-Zn-N_4	154.7	N_2-Zn-N_3	82.2
N_4-Zn-N_3 + N_4-Zn-N_1 + N_1-Zn-N_2 + N_2-Zn-N_3 = 359.9		N_4-Zn-N_3 + N_4-Zn-N_1 + N_1-Zn-N_2 + N_2-Zn-N_3 = 373.3	

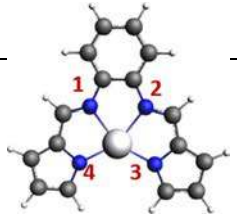

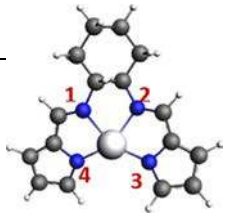

While high conversions (85–98%) and good yields (67–86 %) are obtained with flexible pentacoordinated Zn-N_5SB complexes such as **Zn-1** and **Zn-2** (Table 11, Entries 2–7), the use of rigid Zn-NSB dimers, **Zn-3** and **Zn-4,** slightly improves the selectivity but decreases the cyclic carbonate yields (62-75%, except for entry 11). This activity drop could be explained by the necessary first step formation of the corresponding monomeric species in the reaction media, which may be the real catalytic species. The higher catalytic activity of monomeric zinc complexes *versus* dimers or aggregates was already reported for the cycloaddition of CO_2 [42]. Some of us already also showed that the dimeric zinc species (obtained as crystals at room temperature) undergo a dissociation process before acting as active catalyst for the CO_2 cycloaddition to styrene [52,58]. Besides, the Lewis acid character previously estimated with the Mulliken charge analysis (Table 10) shows that the zinc atoms of the **Zn-1** and **Zn-2** monomers are slightly more acidic than those in the **Zn-3**

Table 8
Dimerization energy of Zn-3 and Zn-4 (kJ/mol).

	Zn-3	Zn-4
Dimerization electronic energy	−107.4	−125.8
Dimerization free energy at 273K	−48.9	−70.6
Dimerization free energy at 323K	−39.7	−61.4
Dimerization free energy at 373 K	−30.5	−52.3

Table 10
Mulliken atomic charges of Zn.

Complex	Mulliken Charges
Zn-1	0.854
Zn-2	0.852
Zn-3	*0.811
Zn-4	*0.812

*same value for both zinc centers.

Table 9
Electronic dimerization energy (kJ/mol) according to typical exchange-correlation (XC) XC functionals.

XC	GGA				hybrids		Meta-GGA				Dispersion corrected				
	BLYP	BP86	PBE	RPBE	B3LYP	PBE0	M05	M05−2X	M06	M06−2X	BLYP-D	BP86-D	PBE-D	B97-D	B3LYP-D
Zn-3	−77.3	−93.6	−107.8	−76.9	−92.4	−115.4	43.1	−284.7	135.4	−84.9	−183.5	−186.4	−174.3	−183.9	−185.6
Zn-4	−99.1	−109.1	−125.8	−96.1	−117.5	−136.7	−39.7	−265.4	5.0	−144.2	−213.2	−209.0	−193.3	−214.9	−216.9

*References to functionals are given in the full table given in supplementary material (Table S.5).

Table 11
Zn-nitrogen Schiff base complexes and tetrabutylammonium halides as Lewis acid/base (LA/LB) catalysts for the cycloaddition of CO_2.

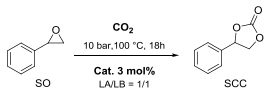

Entry	Zn-NBS	NBu_4X X	Conversion SO (%)	Yield SCC (%)	Selectivity *vs.* SCC (%)
1	–	Cl, Br, I	38	35	92
2		Cl	85	67	79
3	**Zn-1**	Br	97	85	88
4		I	92	78	85
5		Cl	94	82	87
6	**Zn-2**	Br	95	86	91
7		I	98	84	86
8		Cl	76	66	87
9	**Zn-3**	Br	77	71	92
10		I	77	75	97
11		Cl	95	90	95
12	**Zn-4**	Br	73	67	92
13		I	64	62	97

Reaction conditions: SO (2 mmol), LA = LB = 3 mol% *vs.* SO, (0.06 mmol), 5 ml DCM.

Table 12
Catalysts loadings with **Zn-1** complex (LA) and NBu_4Br (LB).

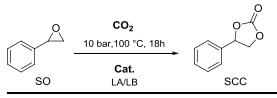

Entry	**Zn-1** mol% [a]	NBu_4Br mol.% [a]	Conversion SO [%]	Yield SCC [%]
1	0	3	30	28
2	1	1	60	50
3	1	3	96 ± 2[b]	91 ± 3[b]
4[c]	1	3	98[c]	97[c]
5	2	2	78	67
6	3	1	37	25
7	3	0	4	0

Reaction conditions: SO (2 mmol), LA or LB (up to 0.06 mmol), 5 ml DCM.
[a] mol % *vs.* styrene oxide.
[b] determined as average values of 4 tests.
[c] 24 h.

and **Zn-4** dimers. Thus the catalytic activity of this zinc complex series may be related to their Lewis acidity: the most acid being the most active ***Zn-1*** = ***Zn-2*** > ***Zn-3*** ≈ ***Zn-4***.

Nevertheless, an exception occurs with the cyclohexyl containing dimer **Zn-4** and NBu_4Cl, (Table 11, Entry 11) leading to the best styrene oxide conversion (95 %) and styrene carbonate selectivity (95 %). As the Cl^- ion has not significant effect on the **Zn-3** phenyl containing dimer, the difference may be due to a structural effect. Thus the *trans*-cyclohexyldiamine bridge, forms less strained, and more stable, helical structure in dimer **Zn-4**. This can be confirmed by the 0.5 Å longer distance between the two zinc atoms in **Zn-4** as compared to **Zn-3**, which is then easier to disaggregate.

A neat influence of the halogen nature of NBu_4X on the catalytic activity is noticed when using complex **Zn-4**: styrene oxide conversion increases with X electronegativity while styrene carbonate selectivity is almost the same (92–97 %). This may suggest that the halogen nucleophilic attack (opening the epoxide) is the rate determining step and varies with the halogen nature (SO conversion) while the formation of the cyclic carbonate (SCC selectivity) seems more related to the Zn(II) Lewis acidity.

As often reported, increasing the amount of ammonium halide favors the efficiency of the combined LA/LB catalysts. [27,34,42,63] Thus, a molar ratio screening was carried out using the new Schiff base complex **Zn-1**, combined to NBu_4Br as catalytic system. Selected results are summarized in Table 12. Using catalysts separately, (Table 12, entries 1 and 7), clearly points out that NBu_4Br is essential in the reaction and that the cooperation between both LA and LB is required to obtain good cyclic carbonate yields, confirming the proposal that the Lewis acidity of the zinc complex improves the ring closing, to form the cyclic carbonate, thus enhacing the cyclic carbonate selectivity.

In order to optimize the catalytic performance, both loadings were varied from 1 to 3 mol% keeping the same molar ratio (LA/LB = 1). Decreasing the catalyst amount *vs.* SO (Table 11, entry 3) from 3 mol% to 2% or 1% (Table 12, entries 2 and 5) declined both, the epoxide conversion and the cyclic carbonate selectivity. Inspired by previous works [27,34,42,63], an excess of Lewis base was tested, and the best results of catalytic activity and selectivity were reached with a three-fold increase on NBu_4Br (Entry 3). In contrast, an excess of Lewis acid (LA/LB = 3/1) gave poor results (Entry 6). Furthermore, the better conditions (LA/LB = 1/3) were tested four times leading to a slight variation of SO conversions and SCC yields (± 3%), demonstrating the reproducibility of the system under conditions of entry 3. Thus, a **Zn-1**/NBu_4Br molar ratio of 1/3, 10 bar of CO_2 and 100 °C were selected for following of the study.

2.3. Time and temperature effects

Reaction time is also an important parameter: increasing it to 24 h (Table 12, entry 4) allowed an almost complete cycloaddition of styrene oxide catalyzed by the **Zn-1**/NBu_4Br system with 98 % conversion and 97 % styrene cyclic carbonate yield. On the other hand, shortening reaction time to 6 h reduced both SO conversion and % SCC yield to 57 and 51 %, respectively. This short reaction time was used to evaluate the influence of the temperature on the catalytic results (Fig. 9a). The increase of yield and selectivity towards styrene cyclic carbonate with temperature points out that SCC is a thermodynamic product with significant activation energy, whereas polycarbonate by-product is a kinetic one, in accordance with a previous work [64]. The temperature dependence observed also explains the evolution of the selectivity with the reaction time at 100 °C (Fig. 9b). No product is formed during the heating period (~15 min), *i.e.* until the reaction medium is reaching the selected temperature through the autoclave thick steel walls. As soon as the reaction mixture temperature is attained (T = 100 °C) reaction time is equal to zero (t = 0). Then, the cyclic carbonate begins to form and increases with time, while the selectivity remains almost unchanged. Therefore, the process is very selective to cyclic carbonate as soon as the reaction temperature is high enough to overcome this product activation energy, since SCC is the thermodynamic product.

In order to obtain additional information, the evolution of styrene oxide molar concentration with time was studied (Fig. 10a). The linear plot of ln([SO]) *versus* time (Fig. 10b) indicates that styrene oxide follows a first order rate and the k value was determined: k = 3.80E-05 s^{-1}. Moreover, it is possible to get some information about the thermodynamics of the process using this value of k and the Eyring equation ($k = [k_BT/h]\exp[\Delta G^{\ddagger}/RT]$) to estimate the Gibbs energy of activation $\Delta G^{\ddagger}$ in the range of 120 kJ/mol. This moderate ~30 kcal/mol value of $\Delta G^{\ddagger}$ confirms that energy is needed to form the cyclic carbonate, which is in agreement with the dependence on temperature reported before (Fig. 9a).

3. Reactants effects

3.0.1. CO_2 pressure

In order to evaluate the effect of reactant concentrations, short tests were carried out, to avoid complete SO conversion, which enables to better observe differences in styrene oxide conversions and styrene

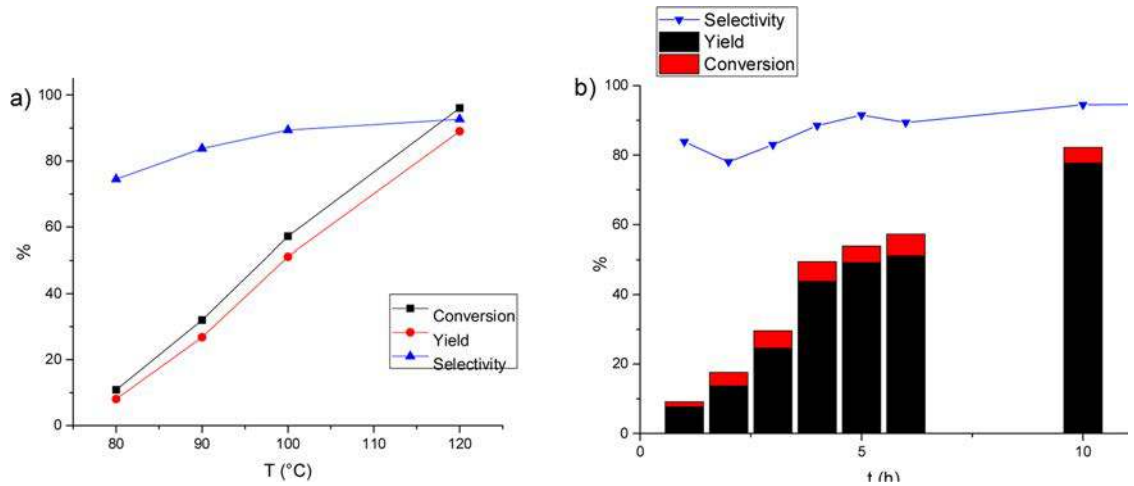

Fig. 9. Conversion and yield **a)** *versus* temperature at 6 h; **b)** *versus* time at 100 °C.
Other Reaction conditions: SO (2 mmol), **Zn-1** = 1 mol%, NBu_4Br = 3 mol%, 10 bar CO_2, 5 ml DCM

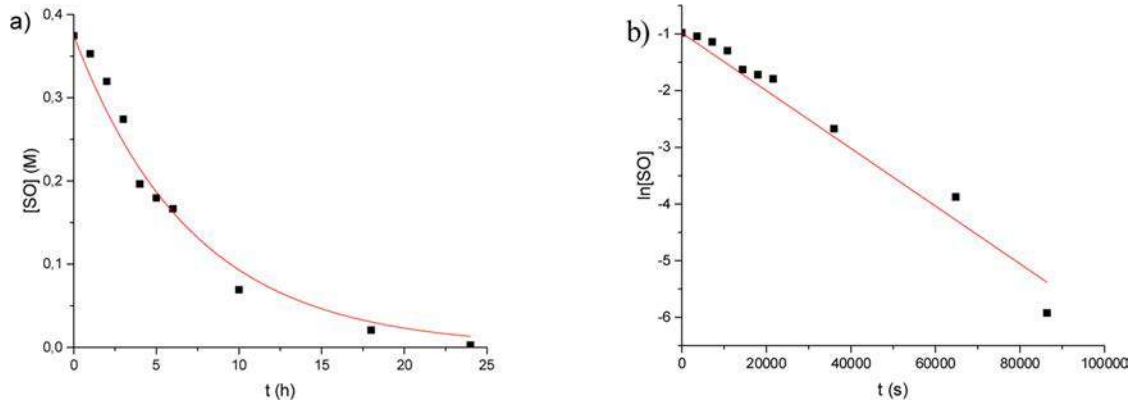

Fig. 10. a) Evolution of [SO] with time and b) ln([SO]) *versus* time.
Reaction conditions: SO (2 mmol; 0.4 M), 5 ml DCM, **Zn-1**(1 mol%), NBu_4Br (3 mol%) 10 bar CO_2, 100 °C

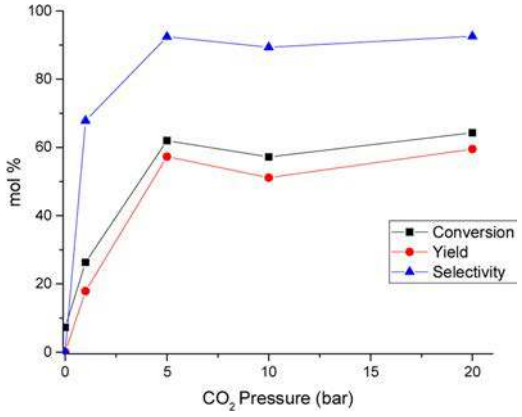

Fig. 11. Effect of CO_2 pressure.
Reaction conditions: SO (2 mmol), **Zn-1** = 1 mol%, NBu_4Br = 3 mol%, 5 ml DCM, 6 h

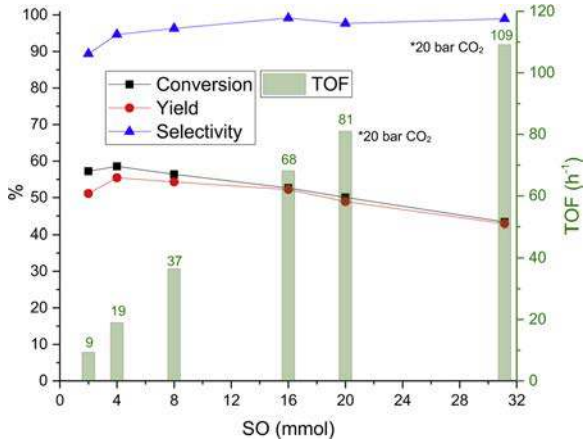

Fig. 12. Effect of styrene oxide concentration on turnover frequency (TOF calc. *vs.* Zn complex) Reaction conditions: **Zn-1** (0.02 mmol), NBu_4Br (0.06 mmol), 100 °C, 6 h, 5 ml DCM, mesitylene as internal standard, 10 (or *20) bar of CO_2.

cyclic carbonate yields. The dependence on pressure was studied varying the initial CO_2 pressure, *ie* the value reached when pressurizing the autoclave at room temperature. Various tests were realized with increasing the CO_2 pressure up to 20 bar (Fig. 11). Without adding CO_2, some phenyl-1,2-ethanediol (2%) is formed by the opening of the epoxide. Then, cyclic styrene carbonate yield improves along with CO_2 pressure. Within a 5–20 bar pressure range, reactivity shows no significant differences, leading up to 64 % SO conversion and 60 % SCC yield. Nevertheless, when using only 1 bar of CO_2, a drastic drop in catalytic activity is observed, due to the lack of CO_2 in the reaction medium, because, at that pressure, only 1.6 mmol of CO_2 are introduced in the 40 ml reactor. The minimal pressure needed to react with 2 mmol of styrene epoxide is about 1.2 bar, considering that CO_2 is very soluble in the solvent (DCM) containing 2 mmol of SO. Thus, at 100 °C, if enough CO_2 is available, the reaction does not depend on pressure and leads to the cyclic carbonate whit high selectivity (up to 94 %).

3.0.2. Styrene oxide loading

Catalytic runs were also carried out increasing the styrene oxide concentration from 2 to 30 mmol keeping constant the solvent volume (5 mL), temperature (100 °C) and catalytic amounts: **Zn-1** (1 mol%) and NBu_4Br (3 mol%). Starting pressure was unchanged (10 bars), except for the tests using large amounts of SO, since more than 10 bar are needed to ensure enough CO_2 when more than 16 mmol of epoxide are introduced in the 40 ml reactor. As shown in Fig. 12, when increasing the epoxide loading, complete cyclic carbonate selectivity is rapidly reached (up to 99 %). Even if the styrene conversion slightly diminishes (from 57 to 43 %), the catalytic system is more active since a linear increase of the turn over frequencies TOF (calc. *vs*. zinc complex: green bars in Fig. 11) is observed, thus confirming the first order rate *vs.* the epoxide. Moreover, if no solvent is added to 31 mmol of SO (3.5 mL), the TOF value significantly improved (Table 13) to reach 232 h^{-1} at 120 °C, suggesting that the solubility of reactants and catalyst is a crucial factor in the CO_2 cycloaddition to epoxides. Under these conditions, the turn over number (TON) increased to 1400 mol of SO per mol of **Zn-1** and the complex loading decreased to 0.06 mol % *vs.* epoxide.

3.1. Reusing test

In order to evaluate the robustness and activity of the new **Zn-1** catalyst over long periods, reusing tests were realized over four days, with 2 mmol of styrene oxide and 10 bar of CO_2 and NBu_4Br (3/1), at 100 °C. After the first 24 h run (Table 12, entry 4), the same amount of styrene oxide was added to the reaction mixture after cooling down, depressurizing and sampling. This procedure was repeated 3 times, and the catalyst didn't lose any activity since complete conversion and selectivity was obtained in each of the following runs. Then, reusing was tested with a ten times fold epoxide loading (20 mmol): after the first 24 h run, 90 % conversion was reached and 88 % yield of cyclic carbonate, and almost the same values were obtained through the week, affording TON values of 3332 calc. *vs*. zinc complex (or 1110 calc. *vs*. ammonium halide). These encouraging results prove that the **Zn-1**/ NBu_4Br (1/3) is a robust and stable catalytic system that remains active over 4 days, allowing more than one thousand styrene oxide molecules to be converted selectively in styrene carbonate by the combined catalytic activity of 1 molecule of LB and 3 molecules of zinc LA.

Table 13
Solvent and temperature effect in high SO loading tests.

Entry	DCM (mL)	T (°C)	Conversion SO [%]	Yield SCC [%]	TOF* (h^{-1})
1	5	100	41	40	109
2	0	100	65	64	169
3	0	120	92	90	232

Reaction conditions: SO (31.15 mmol), **Zn-1** (0.02 mmol), NBu_4Br (0.06 mmol), 6 h.
20 bar CO_2; mesitylene as external standard.*Calc. *vs.* Zn complex.

3.2. Reaction scope

To finalize this study, reaction scope was evaluated with various terminal and internal epoxides overnight at 100 °C, and catalyzed with the **Zn-1**/NBu_4Br (1/3) system (Fig. 13). As expected, the reactivity of terminal epoxides is significantly higher than for internal oxides. No CO_2 cycloaddition is observed nor with trans or cis stilbene oxide and for internal oxides almost no cyclic carbonate is formed from cyclohexene oxide, whose reaction forms polyether as self-condensation product. In the case of aliphatic terminal epoxides, the CO_2 cycloaddition improves with the length of the carbon chain: C3 < C4 < C6. This trend is opposite to the one reported in a solvent free reaction, catalyzed with a NBu_4I/pyridine SB-Zn complex, which has indeed a penta-coordination mode [42]. In addition, renewable sourced epoxides such as epichlorhydrin and glycidol, synthesized from glycerol, were also tested, affording the corresponding cyclic carbonate with 99 % and 81 yield respectively. It turns out that the epichlorhydrin Cl atom has a positive effect since its OH analog is less selective and, also, provides better results than those obtained for styrene oxide under the same reaction conditions (Table 12, entry 3: 96 % conv. 91 % yield 95 % sel.). Other studies also describe the solvent free cycloaddition of CO_2 to epoxides, but the gas and catalytic system may be soluble into the epoxide, to avoid lack of reactivity. This happened with the very active NSB-Zn aniline derived complex Lewis acid catalyst, leading to poor yields of cyclic carbonates of butane oxide and epichlorohydrin [41]. Thus, the scope of the epoxides examined here with the pyrrole N_5SB-Zn complex **Zn-1** is in accordance with other studies, concerning the fact that terminal epoxides react more easily with CO_2 to give the corresponding cyclic carbonates, but points out that the solubility of each substrate and catalyst may also be considered.

4. Conclusions

A series of stable pyrrole derived Schiff base ligands and their corresponding Zn(II) complexes were synthetized and fully characterized. In the two new monomers **Zn-1** and **Zn-2** the central triamine unit in the nitrogen Schiff base allows a tetra or penta coordination, as confirmed by the X-ray analysis of complex **Zn-1,** (distorted trigonal bipyramid) and DFT calculations for **Zn-2**, in which the ligands can be tetradentated when using coordinating solvents. The DFT results show that the deformations towards an axial position of the central nitrogen atom of the triamine, involving trigonal pyramid or square pyramid geometries, cost a very small energy, underlining the lability of the ligand in **Zn-1** and **Zn-2**. It is clear that the pseudorotation or turnstile mechanisms of the **Zn-1** or the **Zn-2** complexes are easy, and therefore favorable to the participation of a catalytic process. Moreover, the pentacoordinated N_5 Schiff base ligand in complexes **Zn-1** and **Zn-2** prevents the formation of dimeric species, while in the case of the N_4 Schiff base complexes **Zn-3** and **Zn-4** self-aggregation occurs, leading to chiral helical structures in which each zinc atom adopts a tetrahedral geometry. The four prepared pyrrole Schiff base complexes **Zn-1** to **Zn-4** were tested as efficient Lewis acids catalysts when combined to ammonium halides as Lewis bases, for the cycloaddition of carbon dioxide over styrene oxide. Even if ammonium halides can moderately catalyze this reaction (<40 % conversion) the activity of the combined catalysts significantly improves with cyclic carbonate yield increasing from 35 % in average to 62–90 % when adding any of the four prepared zinc complexes. When combined to NBu_4Br, monomeric species **Zn-1** and **Zn-2** are quite more active than **Zn-3** and **Zn-4** dimers. As the Mulliken charge analysis showed that the **Zn-1** and **Zn-2** monomers have a higher Lewis acidity than the **Zn-3** and **Zn-4** dimers, we can suggest that catalytic activity of this zinc complex series may be related to their Lewis acidity: the most acid being the most active.

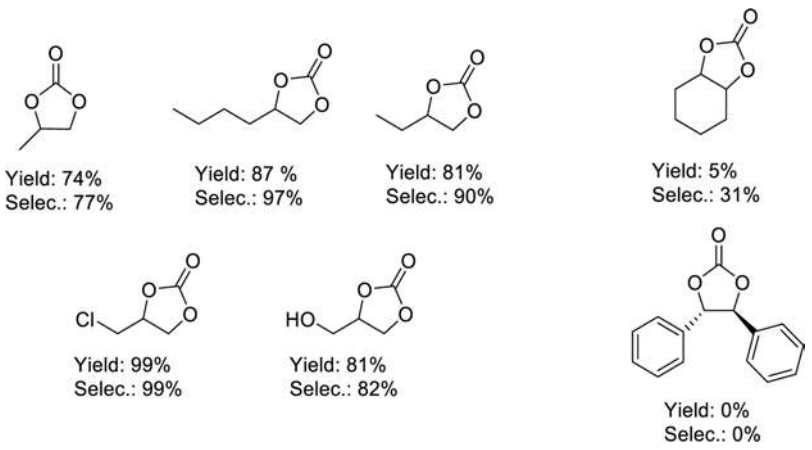

Fig. 13. Epoxide scope.
Epoxide (2 mmol), Zn-**1** (0.02 mmol), NBu_4Br (0.06 mmol), 5 ml DCM, 10 bar CO_2, 100 °C, 18h

As the dimeric species **Zn-3** and **Zn-4**, may undergo a previous decoordination step to form the active catalytic species, structural and thermochemical aspects have been theoretically studied. It is observed that the structure of the monomer derived from **Zn-3,** with phenyl bridge, is perfectly flat whereas the monomer derived from **Zn-4** is more flexible. This geometry deviation is due to the strained structure caused by the chair conformation of the *trans*-cyclohexyl bridge. The calculated dimerization energy shows that the equilibrium monomer-dimer can be easily displaced towards monomers if they are involved in the catalytic cycle, or towards dimers if the crystallization occurs.

The new complex **Zn-1** was chosen as model for an optimization study, pointing out that a two or three fold excess of NBu_4Br improves the catalytic activity of the **Zn-1**/NBu_4Br catalytic system, which is really efficient above 80 °C, thus leading to high styrene oxide conversions (> 90 %). The constant rate of the reaction was determined as well as the corresponding Gibbs energy of activation (~30 kcal/mol), which is in agreement with a strong temperature dependence. Actually, the optimized solvent-free conditions allowed the use of a very small **Zn-1**/NBu_4Br catalyst loading (0.06 and 0.2 mol% respectively) reaching 1400 TON and 232 h^{-1} TOF values at 120 °C (calc. *vs.* Zn complex). The pyrrole Schiff base ligands described here are easier to prepare than their aniline analogs, and their zinc complexes catalytic activities combined to NBu_4Br were confirmed. Moreover, the results obtained at 100 °C in this work (169 h^{-1} TOF) are slightly better than those reported for the aniline derivatives [42,43] (151 h^{-1} TOF) for the solvent-free CO_2 cycloaddition to styrene.

Besides, reusing tests demonstrated that **Zn-1**/NBu_4Br forms a robust catalytic system that remains active over 4 days, allowing the conversion of more than one thousand molecules of styrene oxide to cyclic styrene carbonate by the combined catalytic activity of 1 molecule of Lewis base NBu_4Br and 3 molecules of zinc Lewis acid. Finally, the scope of the reaction was extended to various substrates and very high yields and selectivity were obtained for all the tested terminal epoxides, including epichlorohydrin. As the influence of solubility of the reactants is an important factor, we focus now on screening supercritical CO_2 conditions. Even if catalytic pathways are described with Lewis acids and bases for the cycloaddition of CO_2, we are actually studying the precise mechanism involving NBu_4X and the new pyrrole Schiff base zinc complex **Zn-1**, using a combined experimental and theoretical approach. In addition, as has already reported for other Zn species [55,65], the pyrrole-Schiff base Zn complexes may become bifunctional catalysts, since the central nitrogen atom may form an *in-situ* ammonium salt, thus which may avoid the use of tetrabutyl ammonium halides.

5. Experimental section

5.1. General considerations

All chemicals were purchased from Sigma-Aldrich® and used as received, in particular Et_2Zn as 1.0 M solution in hexanes, styrene oxide (97 %; phenylaldehyde traces) and anhydrous solvents in Sure/Seal ™ bottles. Other solvents were purchased from Across and used without further purification, in particular Carbon dioxide (99.995 % purity) was supplied by Air Liquide. ^1H and ^{13}C NMR spectra were acquired on a Bruker Ascend™ 400 spectrometer and all spectra were acquired at ambient temperature and referenced to the solvent signals [66]; samples were prepared in $CDCl_3$ and acetone-d_6. Infrared spectroscopy analysis was performed with a transformed Fourier IR spectrometer model NEXUS (Nicolet-Thermofisher, UK). Neat samples spectra were recorded in ATR mode with a Thunderdome (Spectratech) accessory containing Germanium crystal with a mono reflection at 45 deg. A DTGS detector was employed, with a 4 cm^{-1} resolution and apodisation Happ-Genzel and 256 scans. Mass spectrometry analysis ESI-HMRS was performed at CCSM-ICBMS à Lyon1 University. Suitable crystals of **Zn-1**, **Zn-3** and **Zn-4** complexes were selected and mounted on a Xcalibur kappa-geometry diffractometer (Rigaku OD, 2018) equipped with an EoS CCD detector and using Mo radiation ($\lambda = 0.71073$ Å). Intensities were collected at 150 K by means of the CrysalisPro software [48]. Reflection indexing, unit-cell parameters refinement, Lorentz-polarization correction, peak integration and background determination were carried out with the CrysalisPro software [67]. An analytical absorption correction was applied using the modeled faces of the crystal [68]. The resulting set of *hkl* was used for structure solution and refinement. The structures were solved by direct methods with SIR97 [69] and the least-square refinement on F^2 was achieved with the CRYSTALS software. [70] All non-hydrogen atoms were refined anisotropically. The hydrogen atoms were all located in a difference map, but those attached to carbon atoms were repositioned geometrically. The H atoms were initially refined with soft restraints on the bond lengths and angles to regularize their geometry (C—H in the range 0.93–0.98 Å) and $U_{iso}(H)$ (in the range 1.2–1.5 times U_{eq} of the parent atom), after which the positions were refined with riding constraints.

NMR, IR and MS spectra and Cartesian coordinates are enclosed in the supplementary information.

5.2. Synthesis of nitrogen Schiff base ligands

L1: To a solution of pyrrole-2-carboxaldehyde (0.644 g, 7.15 mmol) in ethanol (20 mL) at 50 °C, bis(3-aminopropyl)amine (0.5 mL, 3.57 mmol) was added dropwise. The solution was stirred at reflux for 2 h.

Then ethanol was removed under vacuum and the oily product was dissolved in CH_2Cl_2 and washed with water; the organic layer was recovered and anhydrous Na_2SO_4 was added. After filtering, the solvent was removed under vacuum affording **L1** (790 mg, 83 % yield) as an orange oil. ^{1}H NMR (400 MHz, $CDCl_3$): $\delta = 8.08$ (bs, 1 H), 6.82 (bs, 1 H), 6.48 (bs, 1 H), 6.20 b(s, 1 H), 3.60 (bs, 2 H), 2.63 (bs, 2 H), 1.81 (bs, 2 H).

L2: The same procedure used for **L1** was followed, starting from pyrrole-2-carboxaldehyde (0.699 g, 7.15 mmol) and 3,3′-Diamino-*N*-methyldipropylamine (0.5 mL, 3.57 mmol) affording **L2** (840 mg, 90 % yield) as an orange oil. ^{1}H NMR (400 MHz, $CDCl_3$): δ = 8.05 (s, 2 H), 6.86 (s, 2 H), 6.46 (dd, J = 3.5 and 1.3 Hz, 2 H), 6.25 – 6.19 (m, 2 H), 3.54 (t, J =6.5 Hz, 4 H), 2.39 (t, J =7.3 Hz, 4 H), 2.21 (s, 3 H), 1.78 (quint, J = 7.0 4 H).

L3: Pyrrole-2-carboxaldehyde (800 mg, 8.88 mmol) and *o*-phenylenediamine (480 mg, 4.44 mmol) were dissolved in ethanol (20 mL) and stirred at reflux overnight. After cooling, the solvent was removed under vacuum and the crude was dissolved in a minimum quantity of ethanol and hexane was added to recrystallize. The solid formed was recovered by filtration and washed with cold ethanol affording **L3** (728 mg, 63 %) as a pale yellow powder. ^{1}H NMR ($CDCl_3$, 400 MHz): $\delta = 7.73$ (s, 2 H), 7.28−7.23 (m, 2 H), 7.11−7.06 (m, 2 H), 6.42 (dd, J = 1.2 and 3.5 Hz, 2 H), 6.30−6.27 (m, 2 H), 6.04 ppm (dd, J = 2.5 and 3.5 Hz, 2 H) ppm. Similar ^{1}H NMR values in accordance with reported data [49].

L4: The same procedure used for **L1** was followed, starting from pyrrole-2-carboxaldehyde (1500 mg, 16.7 mmol) and (±)-*trans*-1,2-diaminocyclohexane (0.5 mL, 8.33 mmol) affording **L4** (1700 mg, 76 % yield) as a white powder. ^{1}H NMR (400 MHz, $CDCl_3$): $\delta = 7.81$ (s, 1 H), 6.80 (s, 1 H), 6.35 (dd, J = 3.5, 1.3 Hz, 1 H), 6.23 – 6.07 (m, 1 H), 3.14 – 3.04 (m, 1 H), 1.84 – 1.65 (m, 2 H), 1.63 – 1.47 (m, 1 H), 1.45 – 1.29 (m, 1 H). Similar ^{1}H NMR values in accordance with reported data [47].

5.3. Synthesis and theoretical 1H NMR data of Zn-NSB complexes

Zn-1: To a solution of **L1** (790 mg, 2.77 mmol) in THF anhydrous (40 mL) under nitrogen atmosphere, a solution of Et_2Zn (2.90 mL, 2.90 mmol) 1 M in hexane was added dropwise. The solution was stirred overnight at room temperature. After that, the solution was filtered over cotton twice and solvent removed under vacuum. Then, the solid was washed with cold ethanol and hexane, affording the **Zn-1** complex (518 mg 54 % yield) as a pale yellow powder. Suitable crystals were obtained from a solution of dichloromethane and hexane. Melting point: 132−135 °C. ^{1}H NMR ($CDCl_3$, 400 MHz): $\delta = 8.05$ (s, 2 H), 6.92 (s, 2 H), 6.64 (dd, J = 3.3 and 0.8 Hz, 2 H), 6.29 (dd, J = 3.3 and 1.7 Hz, 2 H) 4.06−4.00 (m, 2 H) 3.60−3.53 (m, 2 H), 2.94−2.87 (m, 2 H), 2.60−2.54 (m, 2 H), 2.05−1.96 (m, 2 H), 1.76−1.67 (m, 2 H), 1.46−1.41 (m, 1 H) ppm; ^{13}C NMR ($CDCl_3$, 100 MHz): $\delta = 156.54$, 136.56, 134.04, 113.97, 111.17, 55.41, 50.62, 31.37 ppm. Additionally, theoretical chemical shifts of Zn-1 complex in ^{1}H and ^{13}C NMR spectra is given. ^{1}H NMR Zn-1 spectra (CDCl3, 400 MHz): δ = 8.09, 7.34, 7.07, 6.78, 4.41, 3.80, 3.10, 2.70, 2.36, 1.75, 1.05 ppm; ^{13}C NMR ($CDCl_3$, 100 MHz): δ = 128.72, 125.83, 116.71, 110.94, 92.52, 90.38, 31.15, 13.06. This data show good correlation between observed and predicted proton chemical shifts. However, in the case of theoretical carbon NMR results of studied compounds, all carbons are shifted in comparison to experimental data.

Zn-2: The same procedure used for **Zn-1** was followed, starting from **L2** (840 mg, 2.80 mmol) and Et_2Zn (3 mL, 3 mmol), affording the complex **Zn-2** (734 mg, 72 % yield)) as an orange powder. Melting point: 81 °C. ^{1}H NMR (Acetone-d^6, 400 MHz): $\delta = 8.12$ (s, 2 H), 6.77 (s, 2 H), 6.50 (d, J = 3.3 Hz, 2 H), 6.10 (dd, J = 3.3 and 1.7 Hz, 2 H), 3.81 (s, 4 H), 2.58−2.55 (m, 4 H), 2.01 (s, 3 H), 2.00−1.96 (m, 4 H) ppm; ^{13}C NMR (Acetone-d^6, 100 MHz): δ = 157.83, 134.07, 114.96, 111.62, 59.73, 54.83, 39.27, 27.36 ppm. HRMS (ESI): m/z calcd for $C_{17}H_{24}N_5Zn$ $[M+H]^+$: 362.1323; found $[M+H]^+$: 362.1317. The chemical shifts of protons and carbon observed in Zn-2 complex are: ^{1}H NMR (Acetone-d^6, 400 MHz): $\delta = 7.75$, 6.93, 6.70, 6.39, 3.96, 3.47, 2.61, 2.05, 0.67 ppm; ^{13}C NMR (Acetone-d^6, 400 MHz): δ = 118.54, 114.20, 105.55, 100.22, 80.71, 26.60, 22.08 ppm.

Zn-3: To a solution of **L3** (705 mg, 2.7 mmol) in anhydrous THF under nitrogen atmosphere in a Schlenk flask, a solution of Et_2Zn (2.7 mL, 2.7 mmol) 1 M in hexane was added dropwise and the mixture was stirred at room temperature. After 15 min., the solution turned into a yellow foam and was stirred for 3 h. Then, the foam was dissolved in CH_2Cl_2 and dried under vacuum to give an oil that was dissolved in EtOH. The solid formed by adding hexane was recovered by filtration and dried, affording the complex **Zn-3** (632 mg, 72 % yield)) as a bright yellow solid. Suitable crystals were obtained from a solution of dichloromethane and ethanol. ^{1}H NMR ($CDCl_3$, 400 MHz): $\delta = 7.40$ (s, 4 H), 7.16–7.11 (m, 4 H), 6.89–6.86 (m, 4H), 6.83 (d, J =4.2 Hz, 4 H), 6.53 (s, 4 H), 6.24 (t, J = 1.5 Hz, 4 H) ppm ; ^{13}C NMR ($CDCl_3$, 100 MHz): δ = 153.54, 140.42, 138.30, 137.57, 126.49, 121.28, 120.92, 114.61 ppm. The NMR calculated values for Zn-3 complexe are ^{1}H NMR ($CDCl_3$, 400 MHz): $\delta = 7.69$, 7.46, 7.16, 6.90, 3.26, 1.76 ppm ; ^{13}C NMR ($CDCl_3$, 400 MHz): $\delta = 154.89$, 141.71, 135.03, 117.66, 115.24, 69.57, 40.02, 27.05. Similar experimental and theoretical ^{1}H NMR values are in accordance with reported data [49].

Zn-4: The same procedure used for **Zn-1** was followed, starting from **L4** (256 mg, 0.95 mmol) and Et_2Zn (1 mL, 1 mmol), affording the complex **Zn-4** (100 % yield) as a white powder. Suitable crystals were obtained from a solution of dichloromethane and hexane ^{1}H NMR ($CDCl_3$, 400 MHz): $\delta = 7.30$ (s, 4 H), 7.03 (s, 4 H), 6.75 (d, J = 3.4 Hz, 4 H), 6.42 (dd, J = 3.4 and 1.64 Hz, 4 H), 2.58−2.50 (m, 4 H), 1.64−1.57 (m, 8 H), 1.26−1.09 (m, 8 H) ppm; ^{13}C NMR ($CDCl_3$, 100 MHz): δ = 160.26, 137.52, 134.75, 117.62, 64.80, 37.01, 24.87 ppm. The NMR spectra calculated for Zn-4 complex gives the following results: ^{1}H NMR ($CDCl_3$, 400 MHz): $\delta = 7.80$, 7.78, 7.48, 7.29, 7.22, 7.06, 6.72; ^{13}C NMR ($CDCl_3$, 100 MHz): $\delta = 147.90$, 145.56, 143.97, 138.25, 126.21, 122.71, 117.01. Similar ^{1}H NMR values in accordance with reported data [47].

5.4. Catalytic tests

All the catalytic tests were performed in a 40 ml stainless steel reactor equipped with a thermocouple and stirred with a heating plate. In a typical reaction, 0.06 mmol of the zinc complex and tetrabutylammonium halide, styrene oxide (240 mg, 2 mmol) and mesitylene (120 mg, 1 mmol) used as internal standard, were placed into the autoclave after being weighed. The DCM solvent (CH_2Cl_2) was added and the autoclave closed and directly pressurized with CO_2. The reactor was heated to the desired temperature during the selected time. Then, the autoclave was cooled down to room temperature in an ice bath and depressurized slowly in the hood. The reaction mixture was then analyzed by NMR (300 µl of sample diluted in 700 µl of $CDCl_3$).

5.5. Catalyst reusing tests

Reusing tests were carried using the same procedure as for a standard catalytic test with **Zn-1** (7 mg, 0.02 mmol), NBu_4Br (0.06 mmol, 19.3 mg), styrene oxide (240.3 mg, 2.00 mmol), mesitylene (120.2 mg, 1.00 mmol) and 5 ml of CH_2Cl_2. The autoclave was pressurized with 10 bar of CO_2 and heated to 100 °C. After 24 h, the reactor was cooled down in an ice bath, depressurized and opened to take a sample for analysis (100 µL). The same amounts of styrene oxide (240.3 mg) was added to the reaction mixture before closing, pressurizing and heating the autoclave for the next 24 h (2nd run).

5.6. DFT calculations

DFT calculations were carried out using the Amsterdam Density Functional (ADF) program [71] (2014 and 2016 releases) developed by Baerends and coworkers. [50,51] The PBE gradient corrected exchange-correlation (XC) functional [72], one widely used functional of the GGA family has been herein used for the calculations of the thermodynamics properties, with a Triple Zeta plus Polarization (TZP)

basis set, and with small frozen cores. Relativistic corrections were handled with the ZORA formalism. [73]. The choice of this functional has been validated by a huge amount of calculations on a wide variety of systems, including mainly inorganic, organometallic and solid state systems. See, *e.g.* an extensive benchmark of functional by Mardirossian and Head-Gordon (200 exchange-correlation functionals) [74], and a study of tin complexes [57]. All the structures were characterized by vibrational frequencies calculation in the harmonic approximation, with no imaginary frequency for stable states and a single one for transition states. In order to assess the accuracy of the dimerization energies, several energies calculated with other exchange-correlation functionals have been calculated at the geometries optimized with the PBE functional, through the "meta GGA" ADF [75] keyword, [50] *i.e.* with the PBE electronic densities. The energy convergence and the gradient convergence criteria were set to 1 e -4 a.u. and 2 e-4 a.u., respectively. Before geometry optimizations, the GABEDIT software [76] has been used to draw the starting geometries of the monomers issued from the crystalline structures of the corresponding dimers. Natural bond orbital analysis (NBO) [77] is used to quantify the hybridization. The characteristic of this method makes no a priori assumption about orbital hybridization. The NBO method analyses the electron density or wave function by identifying the most rapidly converging set of NBOs localized orbitals, closely associated with conventional binding concepts. This process involves sequential transformations of atomic orbitals (AOs) to the sets of natural atomic orbitals (NAOs), hybrid orbitals (NHOs), and bond orbitals (NBOs). Weinhold et al., [77] showed that the NHOs are in excellent accord with both electronegativity and bond angle predictions. Therefore, the NBO analysis provides a reliable tool for computational studies of hybridization. In addition, because every NBO is a linear combination of hybrid orbitals, the square of orbital coefficients represents the polarization of the respective bonds in this combination. Thus, the NBO analysis is an ideal theoretical tool for studying the relation between polarization and bond hybridization represented by Bent rule [78].

Credit author statement

All the authors discussed the results. **Miguel Alonso**: experiment achievements, data interpretation, methodology, draft writing. **Lynda Merzoud:** calculations, data interpretation, draft writing. **Walid Lamine**: calculations, data interpretation. **Alain Tuel:** data interpretation, NMR supervision. **Henry Chermette:** calculations, data interpretation, draft writing. **Lorraine Christ**: project initiation, conceptualization, experimental supervision, draft writing. **All authors** contributed to revise the manuscript.

Declaration of Competing Interest

The authors report no declarations of interest.

Acknowledgements

The authors would like to thank Dr. Erwann Jeanneau from Centre de Diffractométrie Henri Longchambon, Villeurbanne, and they gratefully acknowledge the French National Agency (project ANR-OXCY-CAT−CO2) for fundings to realize this work, as well as the GENCI/ CINES for HPC resources/computer time (Project cpt2130), and the PSMN of the ENS-Lyon for computing resources.

References

[1] H. Arakawa, M. Aresta, J.N. Armor, M.A. Barteau, E.J. Beckman, A.T. Bell, J. E. Bercaw, C. Creutz, E. Dinjus, D.A. Dixon, K. Domen, D.L. DuBois, J. Eckert, E. Fujita, D.H. Gibson, W.A. Goddard, D.W. Goodman, J. Keller, G.J. Kubas, H. H. Kung, J.E. Lyons, L.E. Manzer, T.J. Marks, K. Morokuma, K.M. Nicholas, R. Periana, L. Que, J. Rostrup-Nielson, W.M.H. Sachtler, L.D. Schmidt, A. Sen, G. A. Somorjai, P.C. Stair, B. Ray Stults, W. Tumas, Chem. Rev. 101 (2001) 953–996.
[2] M. Aresta, A. Dibenedetto, A. Angelini, Chem. Rev. 114 (2014) 1709–1742.
[3] M. Peters, B. Köhler, W. Kuckshinrichs, W. Leitner, P. Markewitz, T.E. Müller, ChemSusChem 4 (2011) 1216–1240.
[4] T. Sakakura, J.C. Choi, H. Yasuda, Chem. Rev. 107 (2007) 2365–2387.
[5] B. Schäffner, F. Schäffner, S.P. Verevkin, A. Börner, Chem. Rev. 110 (2010) 4554–4581.
[6] M. Tamura, K. Matsuda, Y. Nakagawa, K. Tomishige, Chem. Commun. (Camb.) 54 (2018) 14017–14020.
[7] M. Blain, L. Jean-Gérard, R. Auvergne, D. Benazet, S. Caillol, B. Andrioletti, Green Chem. 16 (2014) 4286–4291.
[8] J.W. Comerford, I.D.V. Ingram, M. North, X. Wu, Green Chem. 17 (2015) 1966–1987.
[9] C. Martín, G. Fiorani, A.W. Kleij, ACS Catal. 5 (2015) 1353–1370.
[10] M. North, R. Pasquale, C. Young, Green Chem. 12 (2010) 1514–1539.
[11] H. Büttner, L. Longwitz, J. Steinbauer, C. Wulf, T. Werner, Top. Curr. Chem. 375 (2017) 50.
[12] P. Yingcharoen, C. Kongtes, S. Arayachukiat, K. Suvarnapunya, S.V.C. Vummaleti, S. Wannakao, L. Cavallo, A. Poater, V. D'Elia, Adv. Synth. Catal. 361 (2019) 366–373.
[13] Y. Chen, P. Xu, M. Arai, J. Sun, Adv. Synth. Catal. 361 (2019) 335–344.
[14] D.J. Darensbourg, Chem. Rev. 107 (2007) 2388–2410.
[15] R.J. Wei, X.H. Zhang, B.Y. Du, X.K. Sun, Z.Q. Fan, G.R. Qi, Macromolecules 46 (2013) 3693–3697.
[16] J.L. Casals-Sainz, A.C. Castro, E. Francisco, A.M. Pendás, Molecules 24 (2019). DOI 10.3390/molecules24122204.
[17] J.E. Del Bene, J. Elguero, I. Alkorta, Molecules 23 (2018) 1–14.
[18] M. Liu, B. Liu, L. Liang, F. Wang, L. Shi, J. Sun, J. Mol. Catal. A Chem. 418–419 (2016) 78–85.
[19] A.R. Hajipour, Y. Heidari, G. Kozehgary, Synlett 27 (2016) 929–933.
[20] X. Gao, M. Liu, J. Lan, L. Liang, X. Zhang, J. Sun, Cryst. Growth Des. 17 (2017) 51–57.
[21] L. He, J.K. Nath, Q. Lin, Chem. Commun. (Camb.) 55 (2019) 412–415.
[22] Y. Wu, X. Song, J. Zhang, S. Xu, N. Xu, H. Yang, Y. Miao, L. Gao, J. Zhang, G. Xiao, Chem. Eng. Res. Des. 140 (2018) 273–282.
[23] J. Liang, Y.B. Huang, R. Cao, Coord. Chem. Rev. 378 (2019) 32–65.
[24] J. Song, Z. Zhang, S. Hu, T. Wu, T. Jiang, B. Han, Green Chem. 11 (2009) 1031–1036.
[25] R. Babu, A.C. Kathalikkattil, R. Roshan, J. Tharun, D.W. Kim, D.W. Park, Green Chem. 18 (2015) 232–242.
[26] Y. Wu, X. Song, S. Xu, Y. Chen, O. Oderinde, L. Gao, R. Wei, G. Xiao, Dalton Trans. 49 (2020) 312–321.
[27] M. North, P. Villuendas, C. Young, Chem. - A Eur. J. 15 (2009) 11454–11457.
[28] X.B. Lu, J.H. Xiu, R. He, K. Jin, L.M. Luo, X.J. Feng, Appl. Catal. A Gen. 275 (2004) 73–78.
[29] F. Jutz, J.D. Grunwaldt, A. Baiker, J. Mol. Catal. A Chem. 279 (2008) 94–103.
[30] P.A. Carvalho, J.W. Comerford, K.J. Lamb, M. North, P.S. Reiss, Adv. Synth. Catal. 361 (2019) 345–354.
[31] A. Decortes, A.W. Kleij, ChemCatChem 3 (2011) 831–834.
[32] J. Meléndez, M. North, R. Pasquale, Eur. J. Inorg. Chem. (2007) 3323–3326.
[33] A. Coletti, C.J. Whiteoak, V. Conte, A.W. Kleij, ChemCatChem 4 (2012) 1190–1196.
[34] X.D. Lang, Y.C. Yu, L.N. He, J. Mol. Catal. A Chem. 420 (2016) 208–215.
[35] Y.M. Shen, W.L. Duan, M. Shi, J. Org. Chem. 68 (2003) 1559–1562.
[36] X. Jiang, F. Gou, X. Fu, H. Jing, J. CO2 Util. 16 (2016) 264–271.
[37] L. Jin, H. Jing, T. Chang, X. Bu, L. Wang, Z. Liu, J. Mol. Catal. A Chem. 261 (2007) 262–266.
[38] L.D. Dias, R.M.B. Carrilho, C.A. Henriques, M.J.F. Calvete, A.M. Masdeu-Bultó, C. Claver, L.M. Rossi, M.M. Pereira, ChemCatChem 10 (2018) 2792–2803.
[39] I. Karamé, M.L. Tommasino, R. Faure, M. Lemaire, Easy Synthesis of New Chiral Tetradentate N4 Schiff Bases and Their Use As Ligands for Metal Complexes, Eur. J. Org. Chem. (2003) 1271–1276.
[40] J.E. Dengler, M.W. Lehenmeier, S. Klaus, C.E. Anderson, E. Herdtweck, B. Rieger, Eur. J. Inorg. Chem. (2011) 336–343.
[41] L. Cuesta-Aluja, M. Djoufak, A. Aghmiz, R. Rivas, L. Christ, A.M. Masdeu-Bultó, J. Mol. Catal. A Chem. 381 (2014) 161–170.
[42] E. Mercadé, E. Zangrando, C. Claver, C. Godard, ChemCatChem 8 (2016) 234–243.
[43] I. Karamé, S. Zaher, N. Eid, L. Christ, Mol. Catal. 456 (2018) 87–95.
[44] E. Rufino-Felipe, N. Lopez, F.A. Vengoechea-Gómez, L.G. Guerrero-Ramírez, M. A. Muñoz-Hernández, Appl. Organomet. Chem. 32 (2018) 1–9.
[45] W.L. Kong, Z.X. Wang, Dalton Trans. 43 (2014) 9126–9135.
[46] L.Y. Yang, Q.Q. Chen, G.Q. Yang, J.S. Ma, Tetrahedron 59 (2003) 10037–10041.
[47] Y. Wang, H. Fu, F. Shen, X. Sheng, A. Peng, Z. Gu, H. Ma, S.M. Jin, J. Yao, Inorg. Chem. 46 (2007) 3548–3556.
[48] J.L.S. Milani, W. de A. Bezerra, A.K.S.M. Valdo, F.T. Martins, L.T.F. de M. Camargo, V.H. Carvalho-Silva, S.S. dos Santos, D. Cangussu, R.P. das Chagas, Polyhedron 173 (2019) 114134–114143.
[49] J.M. Chen, W.J. Ruan, L. Meng, F. Gao, Z.A. Zhu, Spectrochim. Acta - Part A Mol. Biomol. Spectrosc. 71 (2008) 191–198.

[50] K.A. Gerling, N.M. Rezayee, A.L. Rheingold, D.B. Green, J.M. Fritsch, Dalton Trans. 43 (2014) 16498–16508.
[51] W. Lamine, S. Boughdiri, E. Jeanneau, C. Sanglar, C. Morell, L. Christ, H. Chermette, ChemPhysChem 19 (2018) 2938–2946.
[52] W. Lamine, S. Boughdiri, L. Christ, C. Morell, H. Chermette, J. Comput. Chem. 40 (2019) 717–725.
[53] A.W. Kleij, M. Kuil, D.M. Tooke, M. Lutz, A.L. Spek, J.N.H. Reek, Chem. - A Eur. J. 11 (2005) 4743–4750.
[54] M.M. Belmonte, S.J. Wezenberg, R.M. Haak, D. Anselmo, E.C. Escudero-Adán, J. Benet-Buchholz, A.W. Kleij, Dalton Trans. 39 (2010) 4541–4550.
[55] C. Martín, C.J. Whiteoak, E. Martin, M. Martínez Belmonte, E.C. Escudero-Adán, A. W. Kleij, Catal. Sci. Technol. 4 (2014) 1615–1621.
[56] M. Poor Kalhor, H. Chermette, D. Ballivet-Tkatchenko, Ind. Eng. Chem. Res. 59 (2020) 6867–6873.
[57] M.P. Kalhor, H. Chermette, S. Chambrey, D. Ballivet-Tkatchenko, Phys. Chem. Chem. Phys. 13 (2011) 2401–2408.
[58] W. Lamine, S. Boughdiri, L. Christ, C. Morell, H. Chermette, Mol. Phys. 114 (2016) 1066–1075.
[59] H. Abdoul-carime, B. Farizon, M. Farizon, J. Mulatier, J. Dutasta, H. Chermette, Phys. Chem. Chem. Phys. 17 (2015) 4448–4457.
[60] D.J. Darensbourg, S.H. Wei, Macromolecules 45 (2012) 5916–5922.
[61] J. Peng, Y. Deng, New J. Chem. 25 (2001) 639–641.
[62] H. Sun, D. Zhang, J. Phys. Chem. A 111 (2007) 8036–8043.
[63] M. Adolph, T.A. Zevaco, C. Altesleben, S. Staudt, E. Dinjus, J. Mol. Catal. A Chem. 400 (2015) 104–110.
[64] G.P. Wu, S.H. Wei, W.M. Ren, X.B. Lu, B. Li, Y.P. Zu, D.J. Darensbourg, Energy Environ. Sci. 4 (2011) 5084–5092.
[65] S. Sobrino, M. Navarro, J. Fernández-Baeza, L.F. Sánchez-Barba, A. Garcés, A. Lara-Sánchez, J.A. Castro-Osma, Dalton Trans. 48 (2019) 10733–10742.
[66] G.R. Fulmer, A.J.M. Miller, N.H. Sherden, H.E. Gottlieb, A. Nudelman, B.M. Stoltz, J.E. Bercaw, K.I. Goldberg, Organometallics 29 (2010) 2176–2179.
[67] Agilent, Technol. UK Ltd, Yarnton, Oxford, UK, 2014, p. 44.
[68] R.C. Clark, J.S. Reid, Acta Crystallogr. Sect. A 51 (1995) 887–897.
[69] A. Altomare, M.C. Burla, M. Camalli, G.L. Cascarano, C. Giacovazzo, A. Guagliardi, A.G.G. Moliterni, G. Polidori, R. Spagna, J. Appl. Crystallogr. 32 (1999) 115–119.
[70] P.W. Betteridge, J.R. Carruthers, R.I. Cooper, K. Prout, D.J. Watkin, J. Appl. Crystallogr. 36 (2003) 1487.
[71] E.J. Baerends, T. Ziegler, A.J. Atkins, J. Autschbach, D. Bashford, A. Béérces, F. M. Bickelhaupt, C. Bo, P.M. Boerrigter, L. Cavallo, D.P. Chong, D.V. Chulhai, L. Deng, R.M. Dickson, J.M. Dieterich, D.E. Ellis, M. van Faassen, L. Fan, T. H. Fischer, C.F. Guerra, M. Franchini, A. Ghysels, A. Giammona, S.J.A. Van Gisbergen, A.W. Götz, J.A. Groeneveld, O.V. Gritsenko, M. Grüning, S. Gusarov, F.E. Harris, P. van den Hoek, C.R. Jacob, H. Jacobsen, L. Jensen, J. W. Kaminski, G. van Kessel, F. Kootstra, A. Kovalenko, M.V. Krykunov, E. van Lenthe, D.A. McCormack, A. Michalak, M. Mitoraj, S.M. Morton, J. Neugebauer, L. N.V.P. Nicu, V.P. Osinga, S. Patchkovskii, M. Pavanello, C.A. Peeples, P.H. T. Philipsen, D. Post, C.C. Pye, W. Ravenek, J.I. Rodríguez, P. Ros, R. Rüger, P.R. T. Schipper, H. van Schoot, G. Schreckenbach, J.S. Seldenthuis, M. Seth, J. G. Snijders, M. Solà, M. Swart, D. Swerhone, G. te Velde, P. Vernooijs, L. Versluis, L. Visscher, O. Visser, F. Wang, T.A. Wesolowski, E.M. van Wezenbeek, G. Wiesenekker, S.K. Wolff, T.K. Woo, A.L. Yakovlev, S. Theoretical, C. V. U. A. T. Netherlands, Http://www.scm.com, 2016.
[72] J.P. Perdew, K. Burke, M. Ernzerhof, Phys. Rev. Lett. 77 (1996) 3865–3868.
[73] S. Faas, J.G. Snijders, J.H. van Lenthe, E. van Lenthe, E.J. Baerends, Chem. Phys. Lett. 246 (1995) 632–640.
[74] N. Mardirossian, M. Head-Gordon, Mol. Phys. 115 (2017) 2315–2372.
[75] J. Florián, A. Warshel, J. Phys. Chem. B 102 (1998) 719–734.
[76] S. Fias, S. Van Damme, P. Bultinck, J. Comput. Chem. 29 (2008) 358–366.
[77] F. Weinhold, C.R. Landis, Valency and Bonding: A Natural Bond Orbital Donor–Acceptor Perspective, 2005.
[78] H.A. Bent, Chem. Rev. 61 (1961) 275–311.